TECHNISCHE UNIVERSITÄT MÜNCHEN

Institute for
Experimental Physics E21

Annual Report 2008

Annual Report 2008

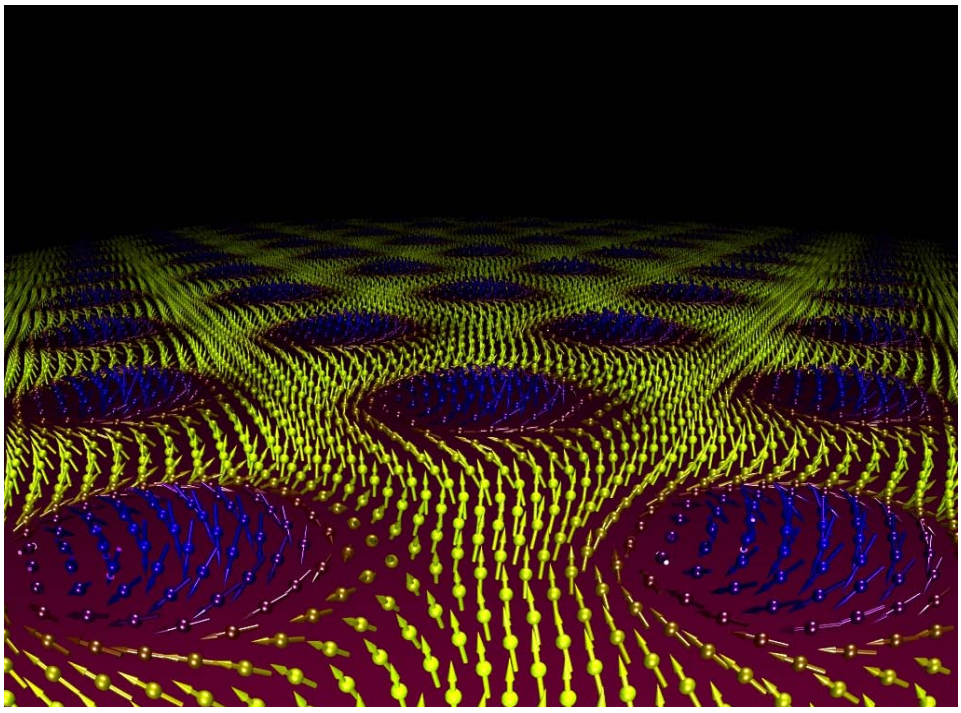

Cover page

Real space depiction of the spin structure of the skyrmion line lattice (section 1.3).

Annual Report 2008

of the Institute for Experimental Physics E21
Prof. Dr. P. Böni
Technische Universität München

Annual Report 2008
of the Institute for Experimental Physics E21
published: July. 2009
Layout by Stefan Legl
Edited by Stefan Legl
http://e21.frm2.tum.de

Technische Universität München
James-Franck-Straße
85747 Garching, Germany

Phone: +49-89-289-14711
Fax: +49-89-289-14713

Contents

Preface

We are pleased to present in the name of the staff of E21 the annual report for the year 2008, which provides an overview on our teaching, research, and development activities. The present report is seriously delayed when compared with previous reports that appeared typically in January. The explanation for the delay is simple and in a sense positive: The year 2008 turned out to be extremely fruitful in terms of the scientific output. Therefore besides our administrative duties, which keep increasing, we were very busy in publishing and preparing presentations in order to distribute our exciting results. In addition, we also spent plenty of time for preparing a preproposal for a Transregio Sonderforschungsbereich in collaboration with Augsburg University and the Ludwig-Maximilians-Universität. It was highly ranked by DFG and we look forward for a positive response when we present the full version to DFG in September 2009.

The year 2008 started successfully with the installation of a new in-pile γ-converter and Pt-moderator inside the positron source NEPOMUC at FRM II rising the intensity of the beam to $(9.0 \pm 0.8)\ 10^8$ moderated positrons per second.
Major breakthroughs emerged from our research projects. For instance, we succeeded to explain major features of the phase diagram of the flux lines in the superconducting phase of niobium and established the emergence of a magnetic skyrmion lattice in the chiral magnet MnSi and its isostructural siblings (see picture on the cover page) by using small angle neutron scattering. These results were only possible thanks to the involvement of highly motivated diploma and doctoral students as well as postdocs and the direct access to the FRM II.
Besides the research at FRM II and in our low temperature and crystal growth laboratories, E21 was bearing a heavy teaching load covering many areas from experimental physics, magnetism, reactor physics, to positron physics. In addition, E21 provided a large number of guided tours through FRM II. Finally on December 15, E21 and E18 organised jointly a special colloquium in honor of Prof. Gläser and Prof. von Egidy on the occasion of their 75^{th} birthday. Both were strongly involved in the operation and research at the 'Atomei'. Last but not least, we also enjoyed many social activities like a bowling evening at the Bürgerhaus in Garching and various BBQs.

Garching, July 2009

Peter Böni Christian Pfleiderer Klaus Schreckenbach

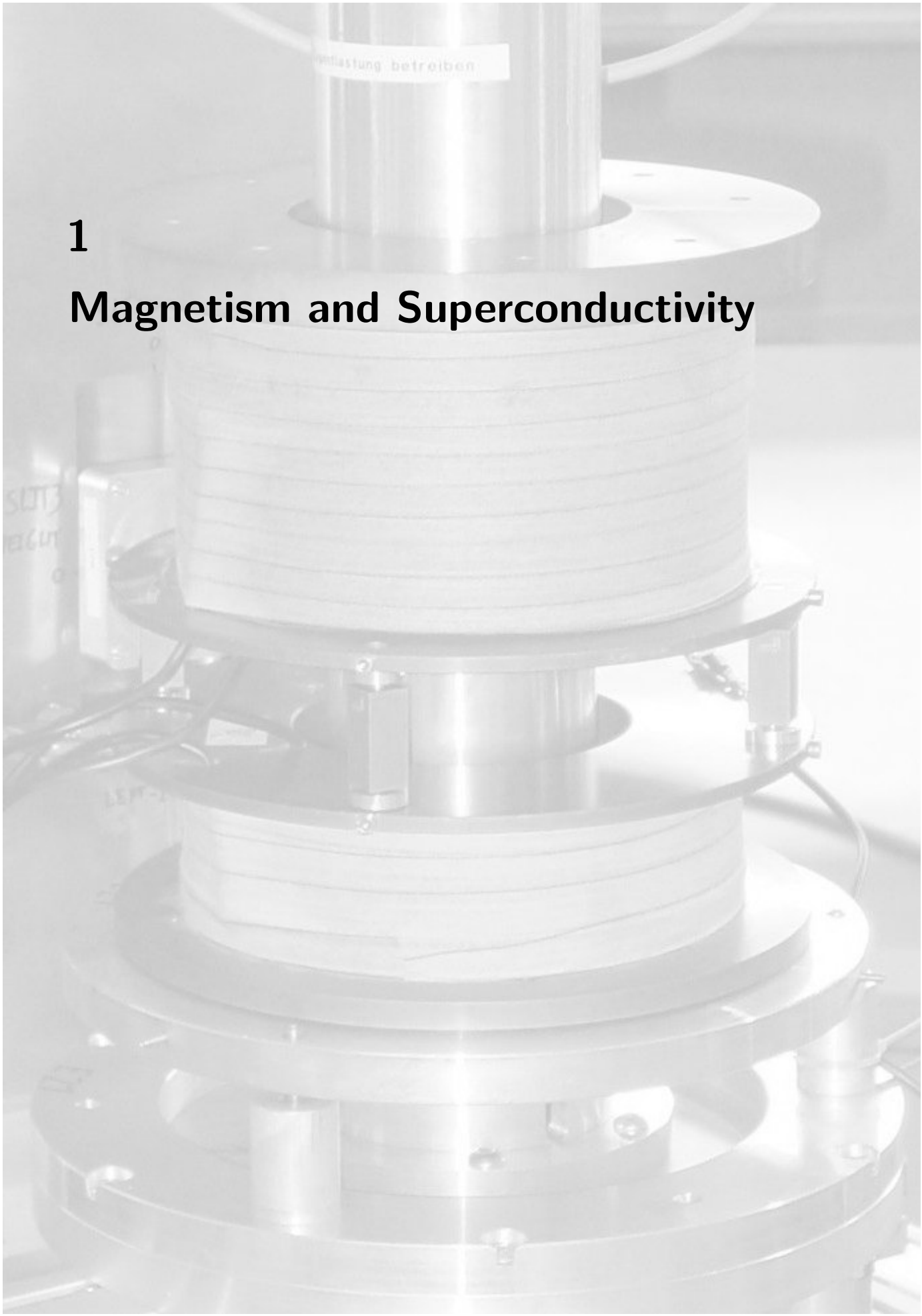

1

Magnetism and Superconductivity

1.1 Nature of the Superconducting Vortex Lattice in Ultra-Pure Niobium

S. Mühlbauer [1, 2], **C. Pfleiderer** [1], **P. Böni** [1], **M. Laver** [3, 4], **E. M. Forgan** [5], **D. Fort** [6], **U. Keiderling** [7], **G. Behr** [8]

[1] *Physik Department E21, Technische Universität München, D-85747 Garching, Germany*
[2] *Forschungsneutronenquelle Heinz Maier-Leibnitz (FRM II), Technische Universität München, D-85747 Garching, Germany*
[3] *NIST Center for Neutron Research, Gaithersburg, Maryland 20899 USA*
[4] *University of Maryland, College Park, Maryland, 20742 Maryland USA*
[5] *School of Physics and Astronomy, University of Birmingham, Birmingham, UK*
[6] *Metallurgy and Materials Science, University of Birmingham, Birmingham, UK*
[7] *Helmholtz Zentrum Berlin, BENSC, D-14109 Berlin, Germany*
[8] *Leibnitz-Institut für Festkörper- und Werkstoffforschung IFW, D-01069 Dresden, Germany*

In the Ginzburg-Landau theory of superconductivity (SC) the formation of a vortex lattice (VL) is the ideal result of the minimization of the Gibbs free energy. Experimental studies have shown [1], that the VL depends sensitively on the microscopic nature, symmetries and number of SC gaps, as well as the general topology of the Fermi surface and the effects of impurities. This raises the question how to generalize the description of VLs. Nb is ideally suited to provide such information. For magnetic field H parallel to a crystallographic $\langle 111 \rangle$ direction the VL in Nb exhibits a hexagonal symmetry. In contrast, for $H \parallel \langle 100 \rangle$, a rich phase diagram unfolds [2, 4, 3]: A two-fold isosceles phase close to T_c and three distinct VL phases at low temperatures are observed. For increasing H at low-T these are a low-field-square phase, a scalene phase at intermediate fields and a high-field-square phase near H_{c2}. Based on the magnetic field dependence, it had been speculated that the low-field-square may be related to the intermediate-mixed-state (IMS) [2]. It had been established that the three low-T phases are tilted with respect to the four-fold symmetry of the underlying crystal structure into a low symmetry direction, thus additionally breaking the crystal mirror symmetry. The two-fold isosceles phase in comparison breaks crystal rotational symmetry but still obeys mirror symmetry. It had also been established that the VL symmetries changes and the tilting vanishes when rotating H away from $\langle 100 \rangle$ until the equilateral VL is recovered for $\langle 111 \rangle$. However, the precise evolution of the VL morphology as a function of field orientation, necessary to identify the nature of the morphology and tilting, remained open.

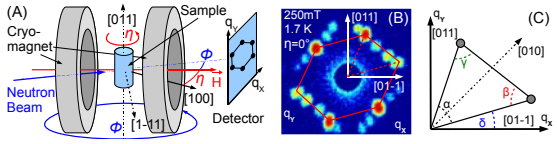

Figure 1: (A) SANS set-up: ϕ denotes the angle between the neutron beam and the magnetic field, while η denotes the angle between magnetic field and the crystal $\langle 100 \rangle$ direction. (B) Typical detector image in the scalene VL phase, one domain is marked red. (C)The nomenclature for describing the VL: α, β and γ represent the internal angles of the FLL unit cell, δ represents the tilting angle of the VL with respect to the horizontal axis.

We report a systematic study of the VL symmetries using small angle neutron scattering (SANS) on the instrument V4 at BENSC, Berlin. To resolve the open issues we have studied an ultra-pure single crystal with RRR $\gtrsim 10^4$, which displays essentially no pinning at all. A sketch of the instrumental setup is given in Fig. 1. We have studied the evolution of the VL morphology for $1.5\,\mathrm{K} < T < 5.5\,\mathrm{K}$, $110\,\mathrm{mT} < H < 330\,\mathrm{mT}$ and $\eta \leq |\pm 25°|$. Typical data is shown in Fig. 2. Our study identifies the low-field-square as a property of the IMS. The remaining VL phases may be viewed as driven by a gradual evolution from an equilateral VL at high temperature and low field to a square VL at low temperature and high field, with a lock-in transition below a magic angle near $\langle 100 \rangle$, where the locked phases are also tilted. The scalene VL thereby appears in transitional regions of high frustration. Our experimental results are consistent with an evolution of non-local corrections in a Eilenberger [5] treatment of a Fermi surface with four-fold symmetry [6]. The magic angle of the transition [8] and the tilting corresponds remarkably well to a change between open and closed Fermi surface sheets, empirically suspected to affect the SC [7].

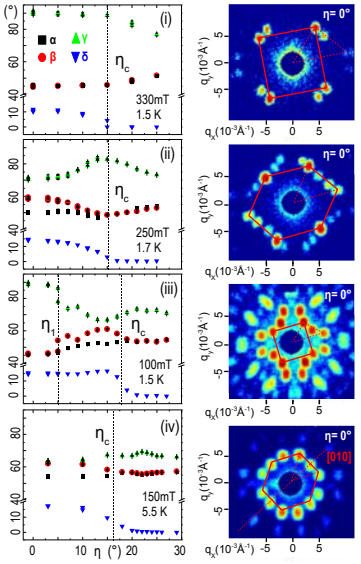

Figure 2: Evolution of the VL as a function of η for various T and H, where typical sums over rocking scans are shown for the high-field-square (i), scalene (ii), low field square (iii) and isosceles (iv) structures. All VL structures are given in reciprocal space, with the angles plotted in the LH panels defined in Fig. 1 [8].

References

[1] A. Huxley et al., *Phys. Rev. Lett.*, 93:187005, 2004.

[2] M. Laver et al., *Phys. Rev. Lett.*, 96:167002, 2006.

[3] M. Laver et al., *Phys. Rev. B*, in review.

[4] D.K. Christen, *Phys. Rev. B*, 21:102, 1980.

[5] G. Eilenberger et al., *Z. Phys.*, 214:195, 1968.

[6] N. Nakai et al., *Phys. Rev. Lett.*, 89:237004-1, 2002.

[7] K.-H- Berthel, dissertation, Dresden, 1976.

[8] S. Mühlbauer et al., *Phys. Rev. Lett.*, 102:136408, 2009.

1.2 Vortex Lattice Dynamics Observed with Time Resolved Stroboscopic Small Angle Neutron Scattering

S. Mühlbauer [1, 2], **C. Pfleiderer** [1], **P. Böni** [1], **E. M. Forgan** [3], **G. Behr** [4], **A. Wiedenmann** [5], **U. Keiderling** [6]

[1] *Physik Department E21, Technische Universität München, D-85747 Garching, Germany*
[2] *Forschungsneutronenquelle Heinz Maier-Leibnitz (FRM II), Technische Universität München, D-85747 Garching, Germany*
[3] *School of Physics and Astronomy, University of Birmingham, Birmingham, UK*
[4] *Leibnitz-Institut für Festkörper- und Werkstoffforschung IFW, D-01069 Dresden, Germany*
[5] *Institut Laue-langevin ILL, Large Scales Group, Grenoble, France*
[6] *Helmholtz Zentrum Berlin, BENSC, D-14109 Berlin, Germany*

In contrast to the local elasticity of crystal lattices, the elasticity of vortex lattices (VL) in superconductors is of non-local origin. The VL elasticity, thermal stability, pinning and transport properties can be described by the temperature, field and k-dependent elastic moduli c_{11}, c_{44} and c_{66}, hence yielding important informations on the microscopic nature of superconductivity [1, 2, 3]. Measurements of the VL elastic moduli are traditionally limited to macroscopic transport measurements on bulk samples or microscopic surface sensitive methods such as decoration or magneto-optical techniques [3, 4].

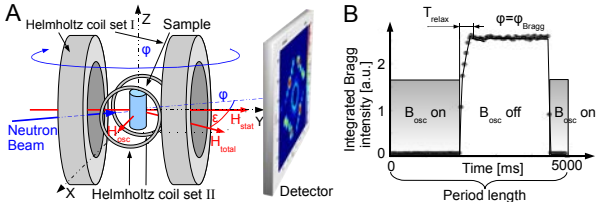

Figure 1: (A) Schematic drawing of the experimental setup: See text for details. (B) Time resolved scan of the VL in niobium switching between two equilibrium positions at 100 mT and 4 K for $\phi = \phi_{Bragg}$, which corresponds to a fullfilled Bragg condition for $\mu_0 H_{osc}$=0 mT. The repetition cycle of H_{osc} was chosen 0.2 Hz with a delay of 1 s, the grey shadowed area corresponds to $\mu_0 H_{osc}$=4 mT. The relaxation towards the Bragg condition for $\mu_0 H_{osc}$=0 mT can be clearly identified. The obtained relaxation time is T_{relax}=500 ms.

We report on a new method to measure the VL tilt modulus c_{44} by means of stroboscopic small angle neutron scattering, combined with a time varying magnetic field setup on an ultra-pure niobium single crystal with vanishing pinning. This method allows the microscopic determination of the intrinsic VL elastic moduli in large bulk samples, unhampered by surface effects. A sketch of the used setup is given in Fig.1: The sample is located in the centre of two orthogonal magnetic fields $\vec{H}_{stat}$ and $\vec{H}_{osc}$, generated by two sets of Helmholtz coils. The resulting magnetic field is $\vec{B}_{total}$, which is inclined by the angle ϵ with respect to $\vec{H}_{stat}$. $\vec{H}_{stat}$ is aligned parallel to the (110) crystal direction of the sample. The neutron beam is oriented approximately parallel to the magnetic field $\vec{H}_{stat}$, whereas the whole setup consisting of both coils and sample can be rocked together around the Z axis by the angle ϕ versus the neutron beam. By applying rectagular pulses on $\vec{H}_{osc}$, the magnetic field direction and therefore the equilibrium position of the VL can be changed, allowing the measurement of the VL relaxation between these different equilibrium positions.

We present first data, showing a clear systematic change of the VL relaxation process as function of temperature, given in Fig.2 for 100 mT 4 K and 6.5 K respectively. Wheras the relaxation at 4 K is characterized by a broadening of the rocking width and a steep step-like increase, followed by a slow relaxation, the 6.5 K plot shows ony one characteristic timescale. The overall relaxation time is reduced, compared to 4 K. Both reduced rocking width and faster relaxation processes with increasing temperature can be explained by the enhanced vortex-vortex interaction due to increasing λ and increased flux flow resistivity respectively. Increasing temperature also leads to faster thermal depinning, furthermore decreasing T_{relax}. Nevertheless, the observed overshoot for 6.5 K remains unexplained for an assumed strongly damped system. The measurements demonstrate, that with the bespoke magnetic field setup combined with stroboscopic SANS, it is possible to access the intrinsic dynamics of bulk VLs on a microscopic scale without the limitations due to imperfections of thin film samples and surface constraints. Relaxation times of the VL between 500 ms for low temperatures and 100 ms close to T_c were measured. The behaviour can be qualitatively explained by increasing thermal depinning and flux-flow resistivity.

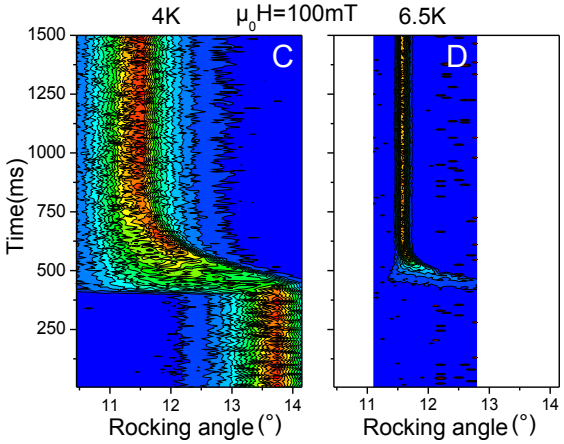

Figure 2: VL rocking curves as function of time for 100 mT 4 K and 6.5 K. The relaxation process between the two equilibrium positions is clearly visible. The scan given in Fig.1 (B) corresponds to a vertical cut at the Bragg angle in (C). Note, that for (D), ony one equilibrium position is shown.

References

[1] A. Huxley et al., *Phys. Rev. Lett.*, 93:187005, 2004.

[2] M. Laver et al., *Phys. Rev. Lett.*, 96:167002, 2006.

[3] E. H. Brandt, *Rep. Prog. Phys.*, 58:1456-1594, 1995.

[4] E. H. Brandt, *Z. Phys. B - Condensed Matter*, 80:167-175, 1990.

[5] K.-H- Berthel, dissertation, Dresden, 1976.

1.3 Skyrmion Lattice in a Chiral Magnet

S. Mühlbauer [1, 2], **B. Binz** [3], **F. Jonietz** [1], **C. Pfleiderer** [1], **A. Rosch** [3], **A. Neubauer** [1], **R. Georgii** [2], **P. Böni** [1]

[1] *Physik Department E21, Technische Universität München, D-85747 Garching, Germany*
[2] *Forschungsneutronenquelle Heinz Maier-Leibnitz (FRM II), Technische Universität München, D-85747 Garching, Germany*
[3] *ITP, Universität zu Köln, Zülpicher Str. 77, D-50937 Köln, Germany*

At ambient pressure and zero applied magnetic field the chiral itinerant-electron magnet MnSi develops helical magnetic order below a critical temperature, $T_c = 29.5\,\mathrm{K}$, that is the result of three hierarchical energy scales. The strongest scale is ferromagnetic exchange favoring a uniform spin alignment. The lack of inversion symmetry of the cubic B20 crystal structure results in chiral spin-orbit interactions, which may be described by the Dzyaloshinsky Moriya (DM) interaction. The ferromagnetic exchange together with the chiral spin-orbit coupling lead to a rotation of the spins with a periodicity λ_h=190 Å that is large compared with the lattice constant, a = 4.56 Å. This large separation of length scales implies an efficient decoupling of the magnetic and atomic structures. Therefore, the alignment of the helical spin spiral along the cubic space diagonal $\langle 111 \rangle$ is weak and is only fourth power in the small spin-orbit coupling. These crystalline field interactions, which break the rotational symmetry, are by far the weakest scale in the system.

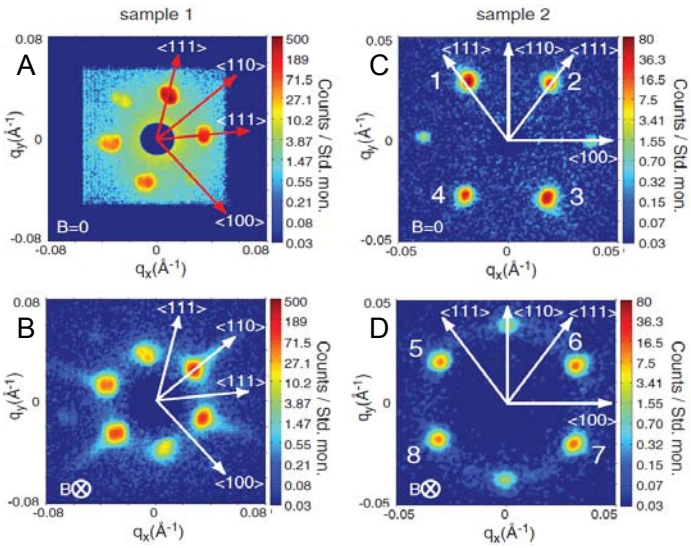

Figure 1: Typical neutron scattering patterns of MnSi: Panel A and C show the known helical state at zero ambient field, where the propagation vector is aligned along the crystalline $\langle 111 \rangle$ direction. Panel B and D show the scattering pattern obtained in the A-Phase. For details see text.

We have performed small angle neutron measurements on MIRA, FRM II to examine the detailed structure of the so-called A-phase, a phase pocket close to T_c at $1/2B_{c2}$, where the propagation vector $\mathbf{Q}$ of the helical order aligns perpendicular to the applied magnetic field. By applying the magnetic field parallel to the incoming neutron beam, we unveiled the complete structure of the A-phase: As shown in Fig. 1, panels B and D, the A-phase is characterized by a regular, sixfold scattering pattern remeniscent of a vortex lattice. This peculiar structure aligns strictly perpendicular to the applied magnetic field, regardless of the underlying crystal symmetry direction. If the scattering plane containes a crystalline $\langle 110 \rangle$ direction, weak pinning is observed.

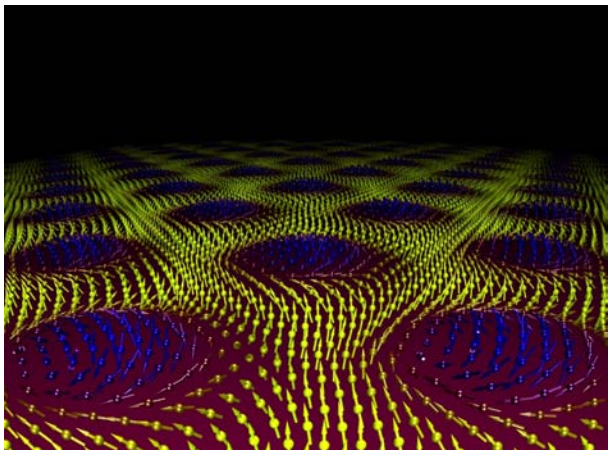

Figure 2: Real space depiction of the spin structure of the skyrmion line lattice. Note that the depiction shows a cut through the skyrmion line lattice in a plane perpendicular to the applied magnetic field.

This structure was indentified as triple-$\mathbf{Q}$ state. A spin-crystal composed of the superposition of three helices under 120° but perpendicular to the magnetic field. The free energy of the triple-$\mathbf{Q}$ state was calculated by means of a Ginzburg-Landau ansatz and found to be metastable. By including Gaussian fluctuations of the form $G \sim F[\mathbf{M}_0] + 1/2 \log\det\left(\frac{\delta^2 F}{\delta \mathbf{M} \delta \mathbf{M}}\right)\Big|_{\mathbf{M}}$ as leading correction to the mean field theory, the free energy of the triple-$\mathbf{Q}$ state was found to have a global minimum. To consider the topology, we compute the winding density of this doubly-twisted magnetic spin crystal $\phi = \frac{1}{4\pi}\mathbf{n} \cdot \frac{\partial \mathbf{n}}{\partial x} \times \frac{\partial \mathbf{n}}{\partial y}$. Integration over one unit cell of the spin crystal yields a skyrmion number $\phi = -1$ per unit cell. Thus a new stable magnetic topology is identified. Topologically stable knots of the magnetisation with particle-like properties arrange themselves in a lattice, which is translation invariant in magnetic field direction. The spin crystal, found in the A-phase of MnSi can be regarded as skyrmion line lattice [1], as shown in Fig. 2.

The skyrmion lattice in the chiral magnet MnSi reported here represents an example where an electronic liquid forms a spin crystal made from topologically non-trivial entities. Our study experimentally establishes magnetic materials lacking inversion symmetry as an arena for new forms of crystalline order composed of topologically stable spin states. This provides a glimpse of the large variety of magnetic states that may be expected from the particle-like magnetic objects currently discussed in the literature.

References

[1] S. Mühlbauer, B. Binz, F. Jonietz, C. Pfleiderer, A. Rosch, A. Neubauer, R. Georgii and P. Böni, *Science*, 323:915 - 919, 2009.

1.4 Geometrically Frustrated Magnetic Systems : Effect of Dimensionality

S. R. Dunsiger [1], **R. F. Kiefl** [2], **G. J. Nieuwenhuys** [3], **P. Böni** [1], **A. Dabkowski** [5], **D. Eschenko** [4], **M. J. P. Gingras** [6], **H. Luetkens** [4], **W. A. MacFarlane** [7], **E. Morenzoni** [4], **J. Preston** [5]

[1] *Physik Department E21, Technische Universität München, D-85747 Garching, Germany*
[2] *Department of Physics and Astronomy, University of British Columbia, Vancouver, V6T 1Z1, Canada*
[3] *Kamerlingh Onnes Laboratory, Leiden University, P.O. Box 9506, 2300 RA Leiden, The Netherlands*
[4] *Laboratory for Neutron Scattering, ETHZ & PSI, CH-5232 Villigen PSI, Switzerland*
[5] *Brockhouse Institute for Materials Research, McMaster University, Hamilton, Ontario, L8S 4L7, Canada*
[6] *Department of Physics and Astronomy, University of Waterloo, Waterloo, Ontario, Canada*
[7] *Department of Chemistry, University of British Columbia, Vancouver, V6T 1Z1, Canada*

Geometric frustration is a widely observed phenomenon in magnetic materials where the crystal structure is based on triangles and tetrahedra and it is hence impossible to satisfy all the magnetic interactions simultaneously. The curiosity about these systems stems from the possibility that if conventional magnetic order is highly frustrated then one may find novel low temperature behaviour. The oxide pyrochlores (general formula $A_2B_2O_7$) are one such example, where the magnetic species sit on the vertices of a three dimensional network of corner sharing tetahedra. In particular, surface μSR measurements [1] have revealed that $Tb_2Ti_2O_7$ is an unusual experimental realisation of a cooperative paramagnet, with only short range spin-spin correlations for all T>0, despite a classical exchange coupling of J$\sim$-13 K. A Low Energy μSR investigation of the internal magnetic fields and Tb^{3+} spin fluctuations in a single crystal of $Tb_2Ti_2O_7$ was undertaken in October 2008, to explore the effect of reduced dimensionality and a surface boundary on the geometrical frustration. It is anticipated that breaking bonds and lattice strain will act to relieve the magnetic frustration. Three slices of a single crystal were cut, polished and annealed such that the $< 111 >$ direction was perpendicular to the surface. In this configuration, the pyrochlore lattice may be viewed as a series of two dimensional kagomé layers of corner sharing triangles separated by sparse triangular layers. Theoretically, nematic order is stabilised on a kagomé lattice, through the mechanism of order-by-disorder [2, 3].

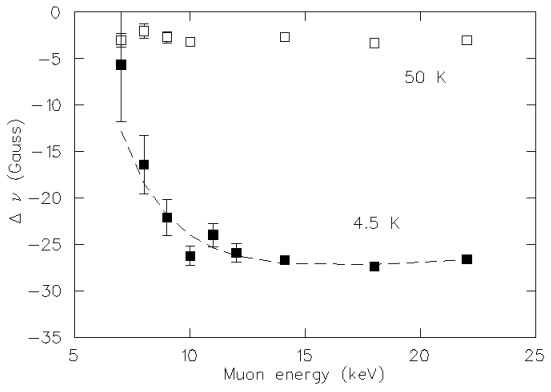

Figure 1: Shift in the muon spin precession frequency at 4.5 and 50 K in $Tb_2Ti_2O_7$ in an applied magnetic field of 100 Oe along the $< 111 >$ direction.

The single crystals, ellipsoidal in shape and which totalled $\sim$160 mm^2 in surface area, were capped with 40nm of Ag, deposited using sputtering techniques. It was thus possible to use higher muon incident energies and yet have the maximum in the implantation profile lie within 10 nm of the metallic Ag / insulating $Tb_2Ti_2O_7$ interface, avoiding known complications arising from backscattering of muons at energies below $\sim$2 keV. As shown in Fig. 1, in a magnetic field applied perpendicular to the sample surface along the $< 111 >$ direction, the paramagnetic shift of the precession frequency in 100 Oe is independent of muon energy at high temperature where short range Tb spin correlations are negligible and agrees quantitatively with the paramagnetic shift observed by bulk μSR, which follows a Curie like temperature dependence [4]. By contrast, at low temperature, where spins are correlated over the lengthscale of a tetrahedron and J$\sim k_B$T, the magnitude of the shift approaches zero as the muon implantation energy is reduced below 15 keV, corresponding to a mean depth of 25 nm into the $Tb_2Ti_2O_7$. The background signal arises from muons which land in the Ag overlayer or miss the sample and land in the backing plate. It should be pointed out that no ordering transition is observed down to 4.5 K.

Complementary measurements undertaken in zero applied field yield evidence for a decrease in the spin lattice relaxation rate T_1^{-1} at low temperatures and implantation energies. In combination, these results suggest that the local susceptibility is smaller, while the Tb spin fluctuations are enhanced close to the interface. The latter is reminiscent of the increase in the spin fluctuation rate observed in the ordered regime of the canonical spin glasses CuMn and AuFe [5] close to the surface and implies this phenomenon may be a more generic feature of frustrated spin systems.

References

[1] J. S. Gardner et al., *Phys. Rev. Lett.*, 82:1012, 1999.

[2] J T Chalker et al., *Phys. Rev. Lett.*, 68:855, 1992.

[3] J N Reimers et al., *Phys. Rev. B*, 48:9539, 1993.

[4] S. R. Dunsiger et al., *Physica B*, 326:475, 2003.

[5] E. Morenzoni et al., *Phys. Rev. Lett.*, 100:147205, 2008.

1.5 Magnetic Fluctuations in Geometrically Frustrated Itinerant Ferromagnets

S. R. Dunsiger [1], R. F. Kiefl [2], P. Böni [1], C. Pfleiderer [1], G. M. Kalvius [1], K. H. Chow [3], W. A. MacFarlane [4], G. D. Morris [5], J. E. Greedan [6]

[1] *Physik Department, Technische Universität München, D-85747 Garching, Germany*
[2] *Department of Physics and Astronomy, University of British Columbia, Vancouver, V6T 1Z1, Canada*
[3] *Department of Physics, University of Alberta, Edmonton, Alberta, T6G 2G7, Canada*
[4] *Department of Chemistry, University of British Columbia, Vancouver, V6T 1Z1, Canada*
[5] *TRIUMF, 4004 Wesbrook Mall, Vancouver, British Columbia, V6T 2A3, Canada*
[6] *Department of Chemistry, McMaster University, Hamilton, Ontario, L8S 4M1, Canada*

Stoichiometric magnetic materials where the crystal structure is based on networks of triangles have been the topic of much interest in recent years as ideal systems for studying the effects of geometrical frustration. In the pyrochlore rare earth and transition metal oxides, of general formula $A_2B_2O_7$, both the A and B magnetic sublattices form a network of corner-sharing tetrahedra. Thus it may not be possible to energetically satisfy all the magnetic interactions simultaneously. The resultant geometric frustration leads to a rich variety of exotic ground states [1]. To date, much of the work has concentrated on local moment systems where novel properties such as cooperative paramagnetism, partial, non-collinear antiferromagnetic ordering, spin-freezing and dipolar "spin-ice' behaviour have been observed.

Latterly, there has been growing interest in the interplay between itinerant and local moments, where the combination of a strongly correlated metal and a geometrically frustrated spin system leads to complex and unusual physical properties. Our collaboration focusses on the metallic pyrochlores $Nd_2Mo_2O_7$ and $Sm_2Mo_2O_7$. $Nd_2Mo_2O_7$ has a ferrimagnetic metallic ground state in which the Mo spin polarised *d* electrons are itinerant while the Nd *f* electrons are viewed as localised [2]. The Mo^{4+} ions undergo a ferromagnetic ordering transition at ≈96 K, where the moments are slightly ($\sim 4°$) canted away from the [100] direction. Subsequently, there is a crossover below roughly 40 K, the Ising like Nd^{3+} ($4f^3$) moments undergoing a partial freezing along the [111] directions to form a "two in and two out' spin ice structure [3]. Neutron diffraction studies [3] indicate the ordered Nd moment size is 1.71(5) μ_B, well below the full moment of 3.5 μ_B anticipated for the free 3+ ion. Hence there must be persistant spin fluctuations well inside the ordered state. This is borne out by μSR measurements taken in a a low longitudinal magnetic field at TRIUMF in June and November 2008 and illustrated in Fig. 1. The measurements of the spin lattice relaxation rate T_1^{-1} on a powder sample show a peak at T_c ∼96 K, accompanied by a rapid drop in the asymmetry consistent with a magnetic ordering transition. No spontaneous precession is observed, indicating a broad distribution of magnetic fields at the muon site(s). T_1^{-1} increases as the ordering temperature is approached from either side, due to critical slowing down of spin fluctuations. A further broad maximum observed around T_g=10 K is associated with a gradual freezing of the Nd spins and a corresponding drop in the bulk magnetisation, as the Nd and Mo moments are approximately antiparallel. However, note that T_1^{-1} is still finite even at 2 K ($T_g/5$), at odds with the behaviour observed in conventional systems undergoing magnetic long range magnetic order.

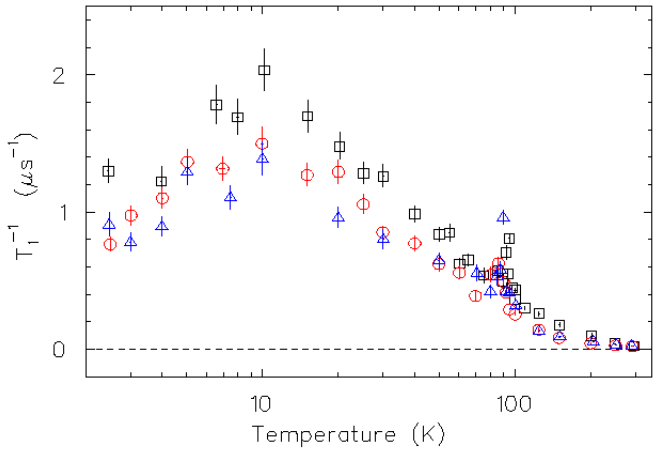

Figure 1: Spin lattice relaxation rate in $Nd_2Mo_2O_7$ (black squares), $Nd_{2-x}Ca_xMo_2O_7$ (red circles) and $Nd_{2-x}Y_xMo_2O_7$ (blue triangles) in a low longitudinal magnetic field (50 Oe).

To our knowledge, no systematic investigation of the relationship between these persistant spin fluctuations and the electrical properties of $Nd_2Mo_2O_7$ has been carried out. We therefore undertook a μSR investigation of T_1^{-1} in powder samples of $Nd_2Mo_2O_7$, $Nd_{2-x}Y_xMo_2O_7$ and $Nd_{2-x}Ca_xMo_2O_7$ as a function of temperature and magnetic field. The Ca introduces hole doping and hence changes the band filling, dilutes the magnetic rare earth species, changing the magnetic interaction channel between the Nd and Mo 4d moments and also introduces disorder. Comparisons with Y substitution are therefore essential, where only the last two mechanisms are relevant. The system is tuned, changing the carrier concentration, *without* changing the ground state. Preliminary results are illustrated in Fig. 1: T_1^{-1} is largest in the unsubstituted compound, while substituting for Nd acts to reduce T_1^{-1}. Initial analysis suggests that the spin lattice relaxation rate in the Ca doped compound is slightly higher than that in the Y substituted analog, where the only effects are due to dilution of the Nd species and the introduction of disorder, but no charge carriers are introduced. This suggests there are indeed changes in the spectrum of spin fluctuations with changing charge carrier concentration.

References

[1] Frustrated Spin Systems, edited by H. T. Diep World Scientific, Singapore, 2004.

[2] N. Ali et al., *J. Solid State Chemistry*, 83:178, 1989.

[3] Y. Yasui et al., *J. Phys. Soc. Jpn.*, 72:865, 2003.

1.6 $NbFe_2$ Single Crystal Growth

A. Neubauer [1], **C. Pfleiderer** [1], **W. J. Duncan** [2], **P. G. Niklowitz** [2], **F. M. Grosche** [3]
[1] *Physik Department E21, Technische Universität München, D-85747 Garching, Germany*
[2] *Dept. of Physics, Royal Holloway, University of London, Egham TW20 OEX, UK*
[3] *Cavendish Laboratory, University of Cambridge, Cambridge CB3 OHE, UK*

Being able to continuously reach a quantum critical point (QCP) in a clean metallic ferromagnetic (FM) system is so far an unresolved question in strongly correlated electron physics. Theoretical considerations argue that a second order FM-QCP cannot be reached. Instead two different scenarios while tuning the transition temperature, by pressure or chemical doping, towards zero are proposed: a first order transition and a transition to a long wavelength modulated magnetic structure [1, 2, 3]. The former has been found experimentally in a number of materials, e.g. MnSi, $ZrZn_2$ and Ni_3Al [4, 5, 6]. The second, the tendency of band ferromagnets to twist, has not been observed so far.

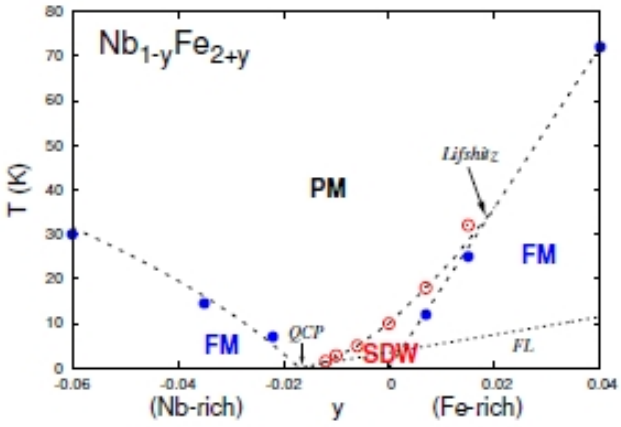

Figure 1: Composition dependent magnetic phase diagram for $Nb_{1-y}Fe_{2+y}$. Starting from the Fe-rich side ($y \geq 0.01$) $Nb_{1-y}Fe_{2+y}$ can be tuned from a FM via a modulated spin-density-wave to a QCP, followed by a FM state.

$NbFe_2$ is a promising candidate for the latter case [7]. By slight variations in stoichiometry $Nb_{1-y}Fe_{2+y}$ can be tuned from a ferromagnetic state via an unresolved magnetic order to a QCP(Fig. 1). Experimental results give rise to the speculation that this unresolved magnetic order of $NbFe_2$ is a, possibly helical, long-period modulated state, also referred to as modulated spin density wave (MSDW). For the stoichiometric case the MSDW forms below a transition temperature of $T_m \approx 10\,K$. Until now, to the best of our knowledge, various attemps to resolve the question of the unknown magnetic state (MSDW) with neutron scattering failed, due to the lack of large homogeneous single crystals.

Using an UHV compatible optical image furnace [8] we prepared six large scale single crystals with different compositions, suitable for neutron scattering experiments. Seed and feed rods were prepared from high purity niobium and iron powder using an UHV cold copper crucible with radiofrequency (RF) heating at Royal Holloway in London. Crystal growth was performed in our 4 - mirror image furnace [8]. Employing counter rotation of the seed and feed rods of 25 rpm and 10 rpm, respectively, and growth rates of 5-8 mm, we successfully grew large single crystals of nominally stoichiometric $NbFe_2$ (Fig. 2). Two high quality homogeneous single crystals ($\cong 2.2$ and $\cong 0.6\,g$) were extracted and extensively characterised. The transition temperatures of the crystals were $T_m \cong 12\,K$ and 6.7 K, indicating a slight Fe and, respectively, Nb accumulation. Motivated by the successful growth of the first two crystals, four $Nb_{1-y}Fe_{2+y}$ crystals with slightly varying compositions (y = -0.007, 0.006, 0.01, 0.018) were grown in the second period (Fig. 2). Varying compositions allow a more detailed investigation of the magnetic phase diagram of $Nb_{1-y}Fe_{2+y}$. First characterisations of the crystals by Laue diffraction show large single crystals areas of several cm.

Figure 2: Overview over the $Nb_{1-y}Fe_{2+y}$ single crystals grown by the vertical-zone-melting technique. Vertical on the left are the 2 crystals grown in the first period with nominally stoichiometric compositon. Horizontally aligned on the right are the 4 crystals with varying composition grown in the second period.

To our knowledge this is the first time large scale single crystals of $NbFe_2$ have been grown using the floating zone technique. We are currently waiting for neutron scattering beamtime to investigate the magnetic order in detail, looking for the first experimental finding of a transition to a long wavelength modulated magnetic structure in the vicinity of a FM-QCP.

References

[1] D.Belitz et al., *Phys. Rev. Lett.*, 82:4707, 1999.

[2] D.Belitz et al., *Phys. Rev. B*, 55:9452, 1997.

[3] A. V. Chubukov et al., *Phys. Rev. Lett.*, 92:147003, 2004.

[4] C. Pfleiderer et al., *Phys. Rev. B*, 55:8330, 1997.

[5] M. Uhlarz et al., *Phys. Rev. Lett.*, 93:256404, 2004.

[6] P. G. Niklowitz et al., *Phys. B*, 72:024424, 2005.

[7] M. Brando et al., *Phys. Rev. Lett.*, 101:6401, 2008.

[8] A. Neubauer et al., see Annual Report 2006 (http://e21.frm2.tum.de).

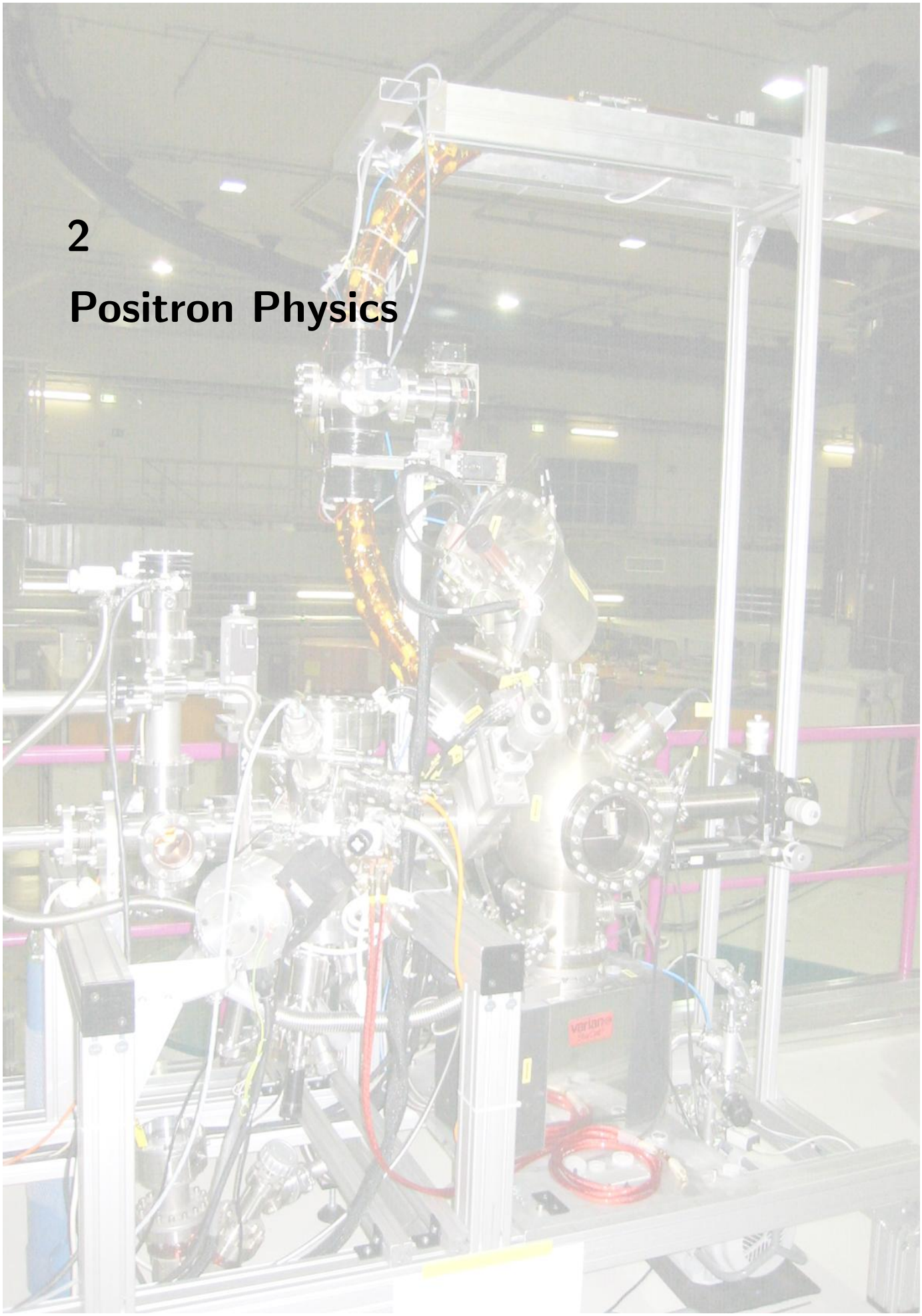

2

Positron Physics

2.1 Unprecedented Intensity of Low-Energy Positrons at NEPOMUC

C. Hugenschmidt [1, 2], G. Dollinger [3], W. Egger [3], G. Kögel [3], B. Löwe [2, 3], J. Mayer [1], P. Pikart [1, 2], C. Piochacz [1, 2, 3], R. Repper [1, 2], P. Sperr [3], M. Stadlbauer [1, 2], K. Schreckenbach [1, 2]

[1] Physik Department E21, Technische Universität München, D-85747 Garching, Germany
[2] Forschungsneutronenquelle Heinz Maier-Leibnitz (FRM II), Technische Universität München, D-85747 Garching, Germany
[3] Inst. für Angewandte Physik und Messtechnik (LRT 2), Universität der Bundeswehr München, D-85577 Neubiberg, Germany

In 2008, a new in-pile γ-converter and Pt-moderator was installed at the neutron induced positron source NEPOMUC. The intensity of the moderated positron beam is unprecedented and amounts to $(9.0 \pm 0.8) \cdot 10^8$ moderated positrons per second at an energy of 1 keV. Hence, the beam facility NEPOMUC provides the world highest intensity of a monoenergetic positron beam reported so far. Up to now, no degradation of the positron yield has been observed for several months of operation. Thus, the long-term stability of the positron beam enables experiments with high reliability.

New In-Pile Source

The design of the new positron source was only little changed in order to eliminate the observed deteriorations of the positron beam. The outer geometry – in particular the Cd-cap for the production of high-energy γ's and the magnetic field coils – remained the same as before. For the new in-pile component, the last Pt-ring was replaced by a Ti-ring which acts as electrical lens as well. Consequently, the lower amount of Pt may lead to an intensity reduction but the beam brightness should increase, since positrons that were emitted from this last Pt-section obtain large transversal momentum that hence mainly contributed to the halo of the beam. In addition, the use of the lighter Ti instead of Pt reduces the γ-heating of the ring-electrodes by about 50%. In order to optimize the heat dissipation to the outer beamtube additional spiral springs at the inner Al-tube guarantee a much better thermal contact.

As previously reported, a small amount of oxygen during reactor operation lead to an increase of the beam intensity which was attributed to the cleaned Pt-surface [1]. The same cleaning procedure with oxygen was first applied for the new source right after the start-up of the reactor in order to clean both, the insulators and the Pt-foils.

During the first months of operation, no degradation of the positron source was observed. The short-term stability of the beam is determined by the variation of the reactor power which is less than 1 %. Due to the long-term stability of the beam, experiments can be performed routinely with an intensity close to 10^9 moderated positrons per second. The beam diameter is the same as at the former in-pile source and amounts to less than 18 mm (full width) in a magnetic guiding field of 6 mT.

Positron Intensity

The positron beam intensity was determined by the detection of the 511 keV γ-radiation of positrons that annihilate at an aluminium target which was moved into the beamline. The background-subtracted γ-spectra obtained for the 1 keV positron beam and of a ^{22}Na reference source, respectively, are depicted in Figure 1. From the analysis of the 511 keV photopeak a beam intensity of $(9.0 \pm 0.8) \cdot 10^8$ moderated positrons per second was deduced. Details of the data analysis taking into account Compton-scattered 1275 keV $\gamma's$ from the reference source, pile-up events, back-scattered positrons and o-Ps-formation with subsequent 3γ-decay are reported elsewhere [2].

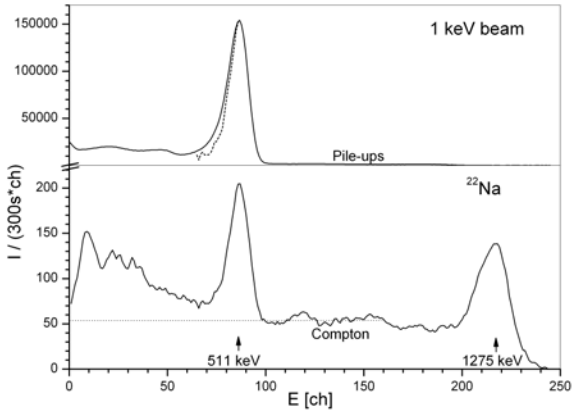

Figure 1: Spectra of the annihilation radiation released from 1 keV positrons annihilating at the target in the beamline. Dashed line in 511 keV photopeak: shape from the ^{22}Na-measurement. Below: Spectrum of ^{22}Na-calibration source for comparison.

Positron Instrumentation at NEPOMUC

A remoderation device for brightness enhancement delivers a 20 eV positron beam (efficiency of about 5%), which is used for all connected experiments, where the beam is additionaly accelerated to the desired energy. Presently, four spectrometers are connected to the NEPOMUC positron beamline: A coincident Doppler broadening spectrometer (CDBS), a positron annihilation induced Auger electron spectrometer (PAES), a pulsed low-energy positron system for positron lifetime measurements (PLEPS), and a set-up for the production of the negatively charged positronium ion Ps^-. The latter experiment is mounted at the multi-purpose beamport, where various experimental set-ups can be connected to the positron beamline. An overview of NEPOMUC and the positron instruments connected to the positron beam facility is given e.g. in [1] and references therein.

References

[1] C. Hugenschmidt, T. Brunner, S. Legl, J. Mayer, C. Piochacz, M. Stadlbauer and K. Schreckenbach, *Phys. Status Solidi C*, 4:3947, 2007.

[2] C. Hugenschmidt, B. Löwe, J. Mayer, C. Piochacz, P. Pikart, R. Repper, M. Stadlbauer and K. Schreckenbach, *Nucl. Instr. Meth. A*, 593:616, 2008.

2.2 High Resolution PAES of the Cu $M_{2,3}$VV-Transition

J. Mayer [1], **K. Schreckenbach** [1], **C. Hugenschmidt** [1, 2]
[1] *Physik Department E21, Technische Universität München, D-85747 Garching, Germany*
[2] *Forschungsneutronenquelle Heinz Maier-Leibnitz (FRM II), Technische Universität München, D-85747 Garching, Germany*

PAES and EAES

Electron induced **A**uger **E**lectron **S**pectroscopy is a conventional method for characterizing sample surfaces in solid state physics. This widely used surface sensitive method probes the first two up to five atomic layers of a sample. But the **P**ositron annihilation induced **A**uger **E**lectron **S**pectroscopy is even more sensitive, since more than 80% of the emitted Auger electrons stem from the topmost atomic layer [1]. Moreover, the secondary electron background in the enery range of the Auger electrons with PAES is considerably reduced compared to EAES. This is caused by the different ionization process which is matter-antimatter annihilation in PAES whereas in EAES the atoms are ionized via impact. Thus, the beam energy of the positrons is maximal $20-30\,\mathrm{eV}$ compared to a few keV with electrons. In summary, PAES is a non destructive, surface sensitive, background free method for surface measurements.

PAES setup at NEPOMUC

The PAES-facility at the FRM-II [2] has been rebuilt in several aspects, most of it due to the newly installed state of the art hemispherical electron energy analyzer. The mean radius of 150 mm and the position sensitive MCP-CCD readout of the electrons enable a higher energy resolution and simultaneously reduce the total measurement time considerably. The elaborate lens design before the entrance of the hemispheres and the pass energy of up to 600 eV enhance the transmission and thus make PAES with positron currents of $\geq 2 \cdot 10^7 \frac{e^+}{s}$ at the sample site feasible.

Measurements

Besides the surface selectivity and the reduction of the secondary electron background the incoming low energy positron does not disturb the electron shell of the atom, which is to be ionized.This is a further advantage of PAES over EAES. Hence, it is possible to get new information about the exact line shape of the Auger transition.
Figure 1 shows the Auger-spectrum of a (100)-copper single crystal (cleaned with Ar^+-ions) excited by a 17 eV-positron beam. Firstly the high signal to noise ratio (SNR) is striking. Compared to conventional EAES (SNR $\approx 1:2$), here the SNR can be estimated conservatively to be at least SNR $\approx 4:1$. PAES-spectra at higher energies than 80 eV showed, that the background drops even below 30 cps, so that the SNR is even an order of magnitude better than with EAES. The higher background results from the backscattered Auger electrons of the Cu_1VV- peak at 105 eV that was not yet studied in detail.

Conclusions

It is the first time that the positron annihilation induced Auger transition of copper with the initial hole in the $3p_{3/2}$ and in the $3p_{1/2}$ shell respectively, is shown with PAES with such a good energy resolution ($< 1\,\mathrm{eV}$) and a first analysis of the lineshape reveals an energy gap of these transitions of $(2.8 \pm 0.08)\,\mathrm{eV}$. Furthermore the measurement time for the spectrum shown in figure 1 was only three hours whereas with other PAES-facilities a spectrum with a worse energy resolution takes several days. A detailed discussion of the Auger-line shape of copper will be published soon.

A further enhancement was the reduction of the measurement time for a rough spectrum from $20-140\,\mathrm{eV}$ to typically less than 15 minutes.

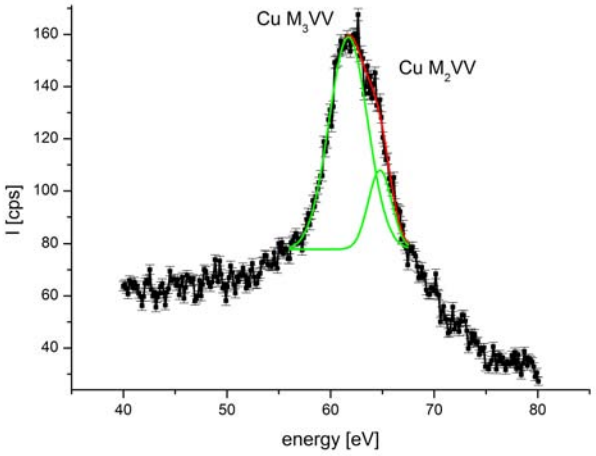

Figure 1: The double peak of the Cu $M_{2,3}$VV*-transition measured with high resolution PAES.*

Outlook

Presently a MCP-phosphor screen assembly at the sample site is installed to improve the focus of the beam. Additionally a grid in front of the MCP will be installed in order to measure (in the absence of magnetic fields) the energy spread of the positron beam at the sample position. Since the new electron energy analyzer is now working properly, measurements of ultrathin metal films or organic molecules on metallic surfaces are planned.

References

[1] K. O. Jensen and A. Weiss, *Phys. Rev. B*, 41:3928-3936, 1990.

[2] C. Hugenschmidt, J. Mayer and K. Schreckenbach, *Surf. Sci.*, 601:2459-2466, 2007.

2.3 Coincident Doppler Broadening Measurement on Thin Tin Layers

P. Pikart [1], **C. Hugenschmidt** [1, 2], **K. Schreckenbach** [1, 2]
[1] *Physik Department E21, Technische Universität München, D-85747 Garching, Germany*
[2] *Forschungsneutronenquelle Heinz Maier-Leibnitz (FRM II), D-85747 Garching, Germany*

Positron annihilation spectroscopy has proved its very high sensitivity to thin tin layers embedded in an aluminium specimen [1]. This high sensitivity is explained by the various trapping effects which cause thermally diffusing positrons to be trapped near the tin-layer (see Fig. 1). The Sn-clusters are expected to be the main attractive trap for positrons due to the high positron affinity of tin (-7.6 eV) compared to aluminium (-4.4 eV). In this project the trapping process is further studied by measuring different material combinations and implantation energies. To date, the existing results could be confirmed with differently grown samples and measurements at various positron energies, corresponding to different mean implantation depths, are shown (see Fig. 3).

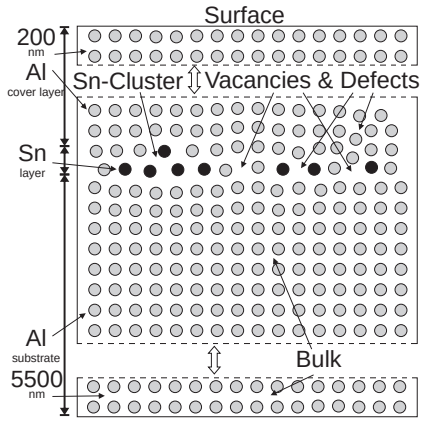

Figure 1: Structure of the layered sample: After implantation, positrons diffuse thermally until annihilation with an electron in the bulk area, or until trapping at a defect site (vacancy, lattice defect or Sn-cluster).

Sample Setup

The new layered samples consist of a 5.5μm thick aluminium substrate, a single 0.1nm tin layer and a top covering layer of 200nm aluminium. Aluminium and tin are thermally evaporated out of high-purity materials on a glass carrier. The thickness of the substrate is choosen so that even positrons of highest energy (30 keV) do not penetrate into the glass carrier, and the thickness of the cover layer is choosen so that medium energy (6 keV) positrons are mainly implanted at its lower border. Since the intermediate tin layer is less than one atomic monolayer, single tin atoms are dispersed or form "nanoclusters" (see Fig. 1).

S over E measurements

The Doppler Broadening (DB) technique allows quick measurements of the S-parameter, which depends on the following features: First the material, second the amount of positrons diffusing back to the surface and third the type and amount of defects in the region of the positron implantation profile. The slope of the S-parameter (see Fig. 2) at low energies is explained by positrons diffusing back to the surface and the much higher S-parameter of the layered system compared to the reference materials is explained by defects caused by the thermal evaporation process.

CDB measurements

The S-parameter in Fig. 2 is steadily increasing in the layered sample, although the implanted tin-atoms should attribute to high-momentum Doppler shifts, which would decrease this value. Hence no tin is visible at simple S-parameter measurements. The Coincident Doppler Broadening technique allows to analyze not only the width of the Doppler Broadening, but also the shape of the broadened photo-peak. By this way each element has its characteristic line shape, and if normalized to a reference spectrum of the substrate (see Fig. 3), these "signatures" can be clearly seen. The tin signature decreases with higher positron energy because the mean implantation depth is shifted below the tin-layer.

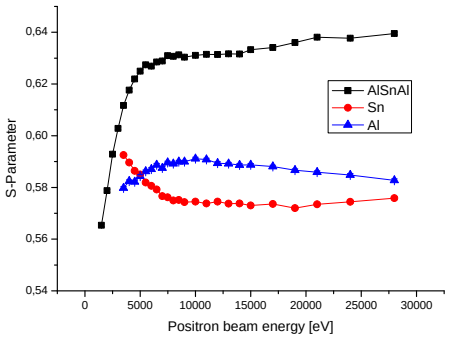

Figure 2: S over E measurement on the layered sample and reference materials.

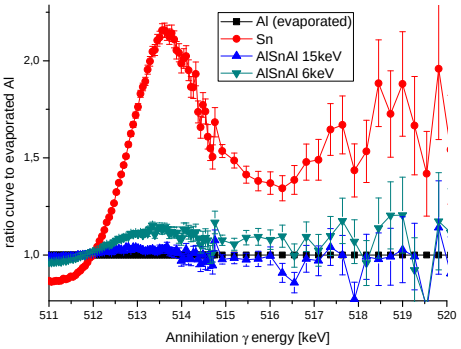

Figure 3: Coincident Doppler Measurement (CDB) of the layered sample and reference materials.

Conclusion

The aluminium-tin layered system has proved its high suitability for fundamental studies of the positron trapping at nanoclusters. Within this project, we plan to perform measurements to analyze different material combinations, to distinguish between effects caused by positron affinity and defect trapping.

References

[1] C. Hugenschmidt, P. Pikart, M. Stadlbauer and K. Schreckenbach, *Phys. Rev. B*, 77:092105, 2008.

2.4 A High Brilliant Pulsed Positron Beam

C. Piochacz [1, 2], **G. Kögel** [3]
[1] *Physik Department E21, Technische Universität München, D-85747 Garching, Germany*
[2] *Forschungsneutronenquelle Heinz Maier-Leibnitz (FRM II), Technische Universität München, D-85747 Garching, Germany*
[3] *Inst. für Angewandte Physik und Messtechnik (LRT 2), Universität der Bundeswehr München, D-85577 Neubiberg, Germany*

Positron annihilation is a highly sensitive method to study defects of atomic size. Both, the types and the concentrations of defects can be determined by positron lifetime measurements. To perform such measurements with micrometer spatial resolution, a pulsed positron beam is focused down to micrometer spot size in the Munich Scanning Positron Microscope (SPM). For a much higher event rate it is intended to operate this SPM at the high intense positron source NEPOMUC at FRM II. Since the beam of NEPOMUC has a smaller phase space density than the beam used in the lab, an interface is under construction, which prepares the beam according to the demands of the last optical column of the SPM. In this interface the DC beam of NEPOMUC is pulsed with a repetition rate of 50 MHz and the energy is raised by newly developed high frequency devices. Moreover, this interface will enhance the beam brilliance [1].

To achieve both, sharp pulses and a high efficiency, the pulsing is done by two different devices. Both perform a linear energy modulation in order to accelerate positrons, which are behind the reference particle and slow down those, which pass too early. After a certain distance the faster positrons will catch up the slower positrons and therefore the positrons drift together to short bunches. The devices differ in the manner the energy modulation is done. The first device is a pre-bunching unit, whose primary aim is not to form very sharp pulses, but to compress as many positrons as possible into a time window of some nanoseconds while the beam is disturbed as less as possible. This buncher utilizes a sawtooth function with a long linear part and therefore it can compress a large amount of the incoming positrons. The following buncher uses a sine function and therefore high amplitudes can be reached by resonant amplification. A further advantage of the sine wave is that the leading and the trailing edge can be used to achieve a small time focus. The disadvantage, that only these positrons could be compressed, which pass the buncher during the small linear parts of the sine wave, is overcome by means of the pre-buncher.

After the successful implementing of this first pulsing components [2] the performance of the pre-bunching unit could be enhanced by a redesign of the HF-excitation of the pre-bunching electrodes. By this improvement, the background could be reduced and the intensity of the pulse was enhanced, while the pulse width is kept as small as before (see Fig 1).

In order to enhance the brilliance of the beam, the interface includes a re-moderator. The setup which is used (see Fig 2), is very similar to that one used for the re-moderator at the NEPOMUC beam facility [3]. After extracting the beam from the magnetic transport field, it is guided electrostatically to a magnetic lens which focuses the beam onto a W(100) single crystal. The positrons, which enter the solid, are scattered inelastically until they reach thermal equilibrium. Now they can diffuse over a distance on the order of 100 nm and some of the thermalized positrons can reach the surface, where they have been implanted. Because tungsten has a negative work function for positrons, those positrons which have reached the surface can leave the solid perpendicular to the surface with a well defined energy. This positrons are formed to a beam by a set of electrodes and guided again electrostatically. Due to the fact that the primary beam and the remoderated beam are on the same axis but propagating in opposite direction they have to be separated by a magnetic dipole. With this setup it was possible to focus the remoderated beam with a long distance electronic lens down to 700 μm.

Due to the installation of the first bunching units and the remoderator, a big step toward the completion of the interface and therefore for the implementation of the SPM was done.

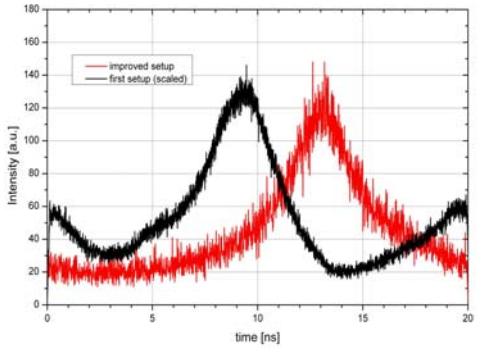

Figure 1: Comparison between the time spectra achieved with the pre-buncher before and after the redesigned HF-exitation.

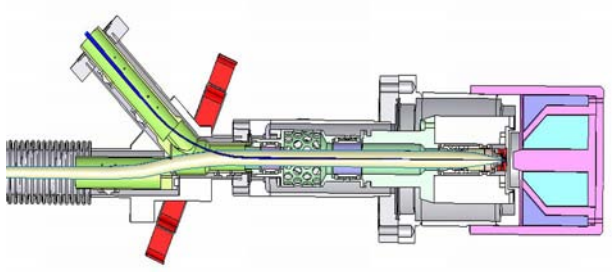

Figure 2: Setup of the remoderator. The primary beam comes from the left side and is indicated by the light yellow tube. The main magnetic dipole field, which is perpendicular to the plane of projection, has a much stronger effect on the slow remoderated beam (blue tube) than on the fast primary beam.

References

[1] C. Piochacz et al., *Physica Status Solidi (c)*, 4:4028-4031, 2007.

[2] C. Piochacz, G. Kögel, W. Egger, P. Sperr and G. Dollinger, Annual Report of E21, 2007.

[3] C. Piochacz et al., *Applied Surface Science*, 255:98-100, 2008.

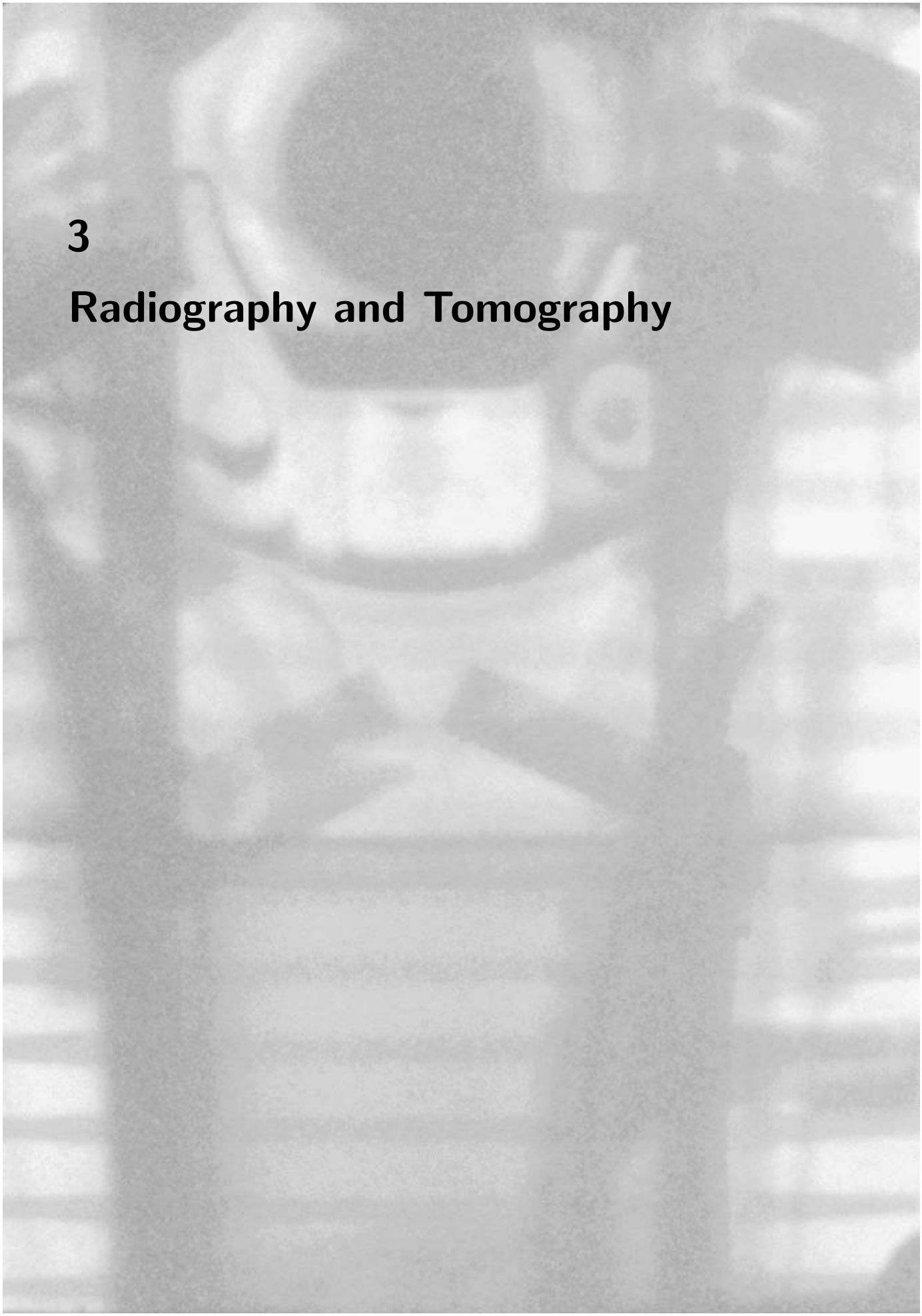

3
Radiography and Tomography

3.1 A Neutron Optical Periscope for Neutron Imaging

B. Schillinger [1, 2], **P. Böni** [1], **E. Calzada** [1, 2], **C. Breunig** [2], **C. Leroy** [3], **M. Mühlbauer** [1, 2], **M. Schulz** [1, 2]

[1] *Physik Department E21, Technische Universität München, D-85747 Garching, Germany*
[2] *Forschungsneutronenquelle Heinz Maier-Leibnitz (FRM II), Technische Universität München, D-85747 Garching, Germany*
[3] *Ecole Centrale Paris, 92 295 Chtenay-Malabry, France*

A standard neutron guide is ill suited for neutron imaging, because the reflections in the guide destroy the collimation of the neutron beam and let the cross section of the neutron guide act like a divergent area source. Most neutron imaging installations use a flight tube instead, but with the direct sight they also have a large background of gamma radiation and fast and epithermal neutrons. With the availability of high-m super mirrors [1], it has now become possible to build a neutron optical periscope that eliminates direct sight with two plain optical reflections only, without destroying the beam collimation ratio. Several prototypes have been built and tested at the ANTARES neutron imaging facility [2, 3]. Several neutron periscopes will be installed during the upgrade of ANTARES in 2009/2010. According to [4], a typical nickel-coated cold neutron guide delivers a collimation of the order of 70 close to its exit, a super mirror guide with $m = 2$ only half of it. The standard selectable collimation ratios of the flight tube setup at ANTARES are 400 and 800. For our first prototype of the periscope, we borrowed four $m = 5$ super mirrors of 0.5m length that were mounted concatenated as two 1 m-mirrors. The maximum intensity of the ANTARES spectrum is at 3.5Å − 4Å, so we assumed a useful wavelength range of 3Å to 5Å. The maximum angle of reflection for the super mirrors is $\lambda \cdot m \cdot 0.1°/\text{Å}$, and thus for 3Å equals 1.5°. Since the periscope must have some angle of acceptance, we defined an angle of 1.2°, so the total angle of deflection was 2.4°. For tests, the periscope was mounted within the measurement chamber of ANTARES, just before the sample position. An entrance window, made of borated polyethylene and lead, limited the incoming beam to the dimensions of the entrance window of the periscope. A beam stop also made of borated polyethylene and lead was mounted within the periscope, blocking the direct beam within. The outgoing beam had a size of $20 \times 58\text{mm}^2$ only and enabled only for the measurements of small samples. If the periscope is mounted close to the reactor, say in 12m distance to the sample, the resulting useful beam height will be 12cm. Fig. 1 shows a sketch of the neutron periscope.

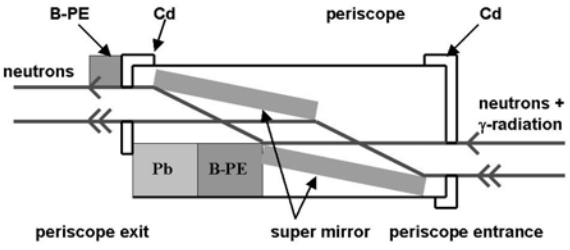

Figure 1: The neutron optical periscope.

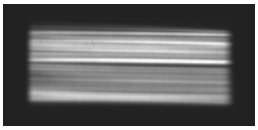

Figure 2: Beam profile transmitted by the periscope.

Measurements

The beam profile transmitted by the periscope shows a striped intensity pattern, resulting from waviness of the mirror caused by imperfect mounting, and surface tension of the coating. A proper glued neutron guide-like mounting will eliminate these inhomogeneities. The open beam measurement shown in Fig. 2 was used to normalize the radiography measurements of a switch and potentiometer as well as a hard disk drive motor shown in Figs. 3 and 4. With these images, it was confirmed that the periscope does not alter the beam geometry on a large scale, other than shifting its axis, and introduced no visible distortion in the images.

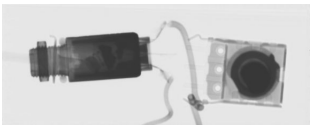

Figure 3: Normalized high-resolution radiograph recorded with the periscope at L/D=800 at ANTARES.

Figure 4: Normalized high-resolution radiograph of a hard disk motor recorded with the periscope at L/D=800 at ANTARES.

Specialized periscopes: Magnetic polarizer and band pass mirrors

The next obvious application was using polarizing mirrors to generate a high-resolution polarized beam. These measurements are reported in a separate report in this issue [5]. Coatings for super mirrors can also be adapted to a desired wavelength range, and can be built to act as band passes. We will next build a matching pair of periscopes that transmit wavelengths shorter than 3.5Å and longer than 4.5Å. With this set, we will be able to perform measurements above and below the Bragg cutoffs of most technical materials. By subtraction of these measurements, the separation of materials from compound work pieces will be possible. Using only the long wavelength band pass will lead to improved transmission through poly-crystalline materials such as steel. All of these periscope types will be incorporated in the upgrade of the ANTARES-II facility in 2010.

References

[1] P. Böni, *NIM A*, 1:586, 2008.

[2] B. Schillinger et. al.,*J.Appl. Rad. Is.*, 61:653-658, 2004.

[3] E. Calzada et. al., *NIM A*, 542:38-44, 2005.

[4] B. Schillinger, *Nondest. Test. Eval.*, 16:141-150, 2001.

[5] M. Schulz et. al., in this issue.

3.2 A Polarizing Neutron Periscope Used for Imaging

M. Schulz [1, 2], **P. Böni** [1], **E. Calzada** [1, 2], **M. Mühlbauer** [1, 2], **A. Neubauer** [1], **C. Pfleiderer** [1], **B. Schillinger** [1, 2]

[1] *Physik Department E21, Technische Universität München, D-85747 Garching, Germany*
[2] *Forschungsneutronenquelle Heinz Maier-Leibnitz (FRM II), Technische Universität München, D-85747 Garching, Germany*

Only recently it has become possible to produce high-m neutron supermirrors. The critical reflection angle Θ_{max} increases linearly with m and is given by $\Theta_{max} = 0.1\ m\ \lambda\,[\text{Å}]$. Currently mirrors with m values up to $m = 4$ are commercially available [1], now also as polarizing supermirrors. This enables for building a neutron polarizing periscope as described in [2] with very high polarizing efficiency for extended beams that leaves the beam collimation untouched, while at the same time eliminating direct sight and thus the gamma, epithermal and fast neutron background. Other polarizing systems like neutron guides or benders would destroy the initial collimation by a large number of reflections, while at the same time introducing intensity inhomogeneities either by the segment joints of a guide or by the multiple plate structure of a bender. A polarizing cavity would not break the direct line of sight and would thus not suppress the background radiation.

Construction

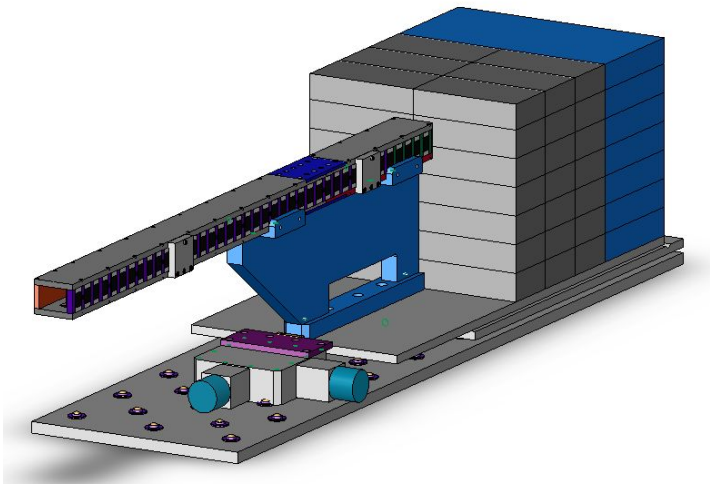

Figure 1: The entire setup with the periscope in the middle and borated PE and Pb block as shielding to stop the primary beam.

Four polarizing supermirrors with a FeSi layer structure of $m = 3.88$ were used to build a first polarizing version of the neutron periscope. They are of 500 mm × 40 mm size each and have a thickness of 2 mm. The periscope was optimized for a wavelength of 3.2 Å, since at this wavelength the neutron flux of a monochromatic beam at the ANTARES facility has its maximum [3]. The mirrors are inclined by an angle of 1° with respect to the incoming beam, allowing to safely reflect a neutron beam with $\lambda = 3.2$ Å and a divergence of 0.1°. The resulting beam width is approx. 17 mm. The height of the beam is approx. 36 mm and is limited by the size of the mirrors. The periscope setup has an overall length of approx. 1.8 m. An overview of the entire periscope assembly as installed at ANTARES can be seen in Fig. 1. A magnetic field of 450 G necessary to saturate the coating of the supermirrors was produced by 200 NdFeB permanent magnets which were arranged on both sides of the polarizer housing, with their magnetization pointing in the same direction. The top and bottom parts of the periscope are made of iron which guides the return field of the permanent magnets to the space where the mirrors are mounted.

Fig. 2 (left) shows a striped structure as already observed in [2], caused by imperfect mounting and surface tension of the mirrors due to the surface coating. The normalised image in Fig 2 (right) shows apparently lower quality than those described in [2]. This is mainly due to the large distance between the sample and the detector (more than 30 cm), caused by the bulky magnetic housing for the ^{3}He polarization analyzer cell for the following experiments. This leads to an inherent blurring of approx 0.4 mm at $L/D = 800$. Fig. 3 shows the polarization that was measured along the horizontal line indicated in Fig. 2 (left).

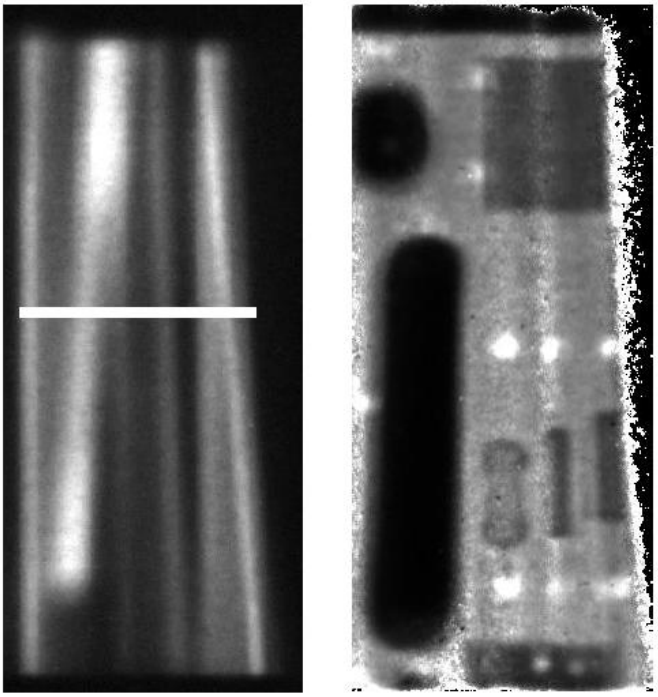

Figure 2: (left): open beam image, the polarization over the white line is shown in Fig. 3; (right): normalized radiograph of a PCB, field of view: approx. 35 × 15 mm^2.

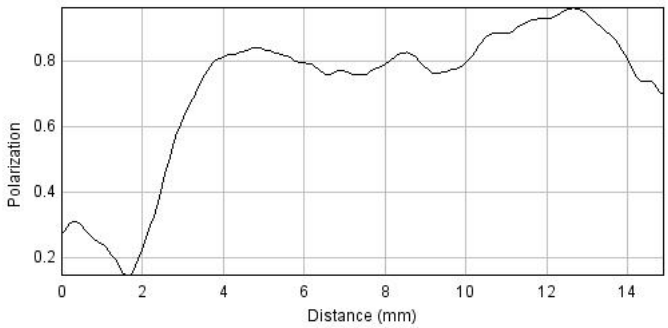

Figure 3: Beam polarization over the line shown in Fig. 2 (left).

With an experimental setup with the periscope as a polarizer and a polarized ^{3}He cell as an analyzer as shown in Fig. 4 it was possible to do first spatially resolved neutron depolarization measurements on ANTARES. This method was used to determine the homogeneity of the concentration of Ni in various Ni_3Al samples. Since the Curie temperature T_C of Ni_3Al depends crucially on the Ni concentration [4], even small deviations from the average concentration over the sample lead to a significant change in T_C. The samples were cylindrical rods (diameter 7 mm, length 50 − 70 mm) cast of molten mixtures of Ni and Al with different concentrations of Ni between 75% and 76% and expected Curie Temperatures of 40 K − 80 K.

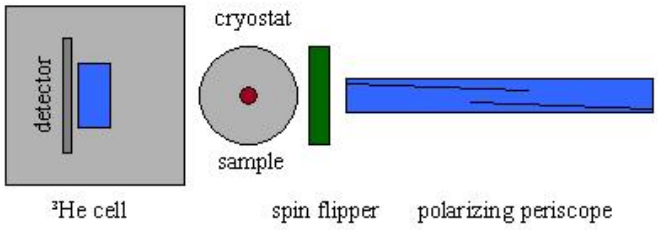

Figure 4: Schematic of the experimental setup.

By changing the sample temperature in a range between 10 K and 90 K (see Fig. 5) it was possible to measure the depolarization of the beam as a function of T.

In the paramagnetic state the beam polarization is not altered by the sample whereas in the ferromagnetic state the beam is depolarized due to the subsequent transmission of magnetic domains with different directions of magnetization [5]. With this method we found that T_C varies in a wide range over the sample volume. In some samples regions could be found where T_C was higher than 100 K, coexisting with regions of $T_C < 10$ K within the same sample. This lets us conclude that the distribution of Ni is inhomogeneous over the samples.

The sample was placed in a closed cycle refrigerator as short a distance away as possible from the magnetic box of a polarized ^{3}He cell analyzer. Thus the minimum sample to detector distance was geometrically constrained to 30 cm, which also limited the maximum resolution to 0.4 mm. Details of this method will be shown elsewhere.

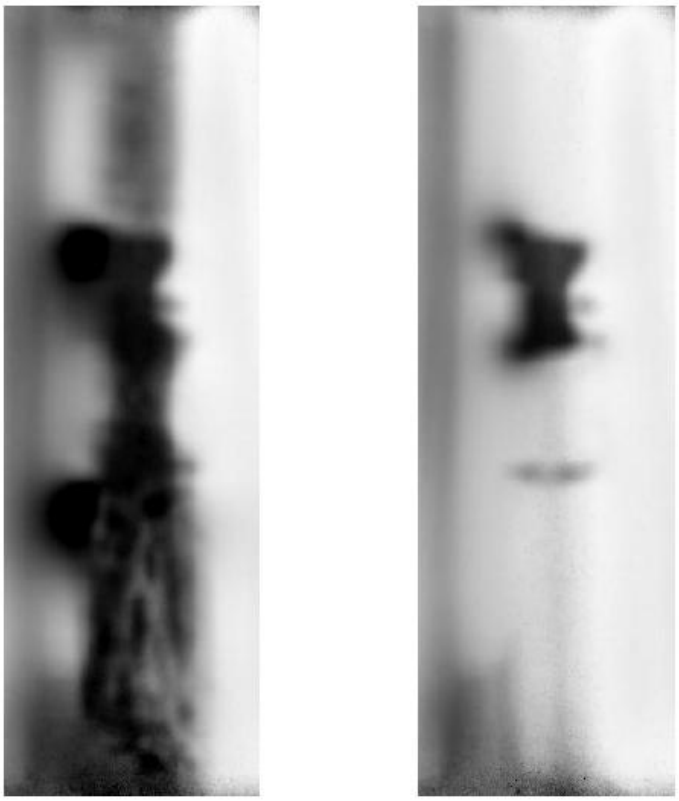

Figure 5: Polarization of a neutron beam after transmission of an OFZ Ni_3Al Sample; white means $P = 1$, black means $P = 0$; (left): 45 K*; (right):* 70 K.

The homogeneity of the beam intensity and polarization can be significantly improved by optimizing the support structures of the supermirrors thus flattening the mirrors. The future polarizing neutron periscopes will be built by the same techniques as a neutron guide. After these improvements we expect a beam polarization of $P \geqq 0.99$ to be feasible.

References

[1] P. Böni, *NIM A*, 1:586, 2008.

[2] B. Schillinger et. al., in this issue.

[3] M. Schulz et. al., acc. pub. NIM A, 2008.

[4] De Boer et. al., *J. Appl. Phys.*, 40:1049-1055, 1969.

[5] O. Halpern and T. Holstein, *Phys. Rev.,* 59:960, 1941.

3.3 New Design for the ANTARES-II Facility for Neutron Imaging at FRM II

E. Calzada [1, 2], **F. Grünauer** [3], **M. Mühlbauer** [1, 2], **B. Schillinger** [1, 2], **M. Schulz** [1, 2]
[1] *Physik Department E21, Technische Universität München, D-85747 Garching, Germany*
[2] *Forschungsneutronenquelle Heinz Maier-Leibnitz (FRM II), Technische Universität München, D-85747 Garching, Germany*
[3] *Physics Consulting, Zorneding, Germany*

Introduction

The ANTARES (Advanced Neutron Tomography And Radiography Experimental System) facility for neutron imaging is successfully operating at the FRM II reactor of the Technische Universität München. In 2009, a redistribution of beam positions at FRM II will require a rebuilding of ANTARES at a different position. The neutron beam SR4b currently hosting ANTARES is the only beam with a cold spectrum that can be extended from the experimental hall of FRM II to the new east hall. ANTARES will have to move to the second channel (SR4a) of the beam tube SR4. Due to the different geometry in relation to the reactor walls, a complete rebuilding of ANTARES is required, including a new shielding concept with lighter materials to meet the restrictions of the permitted floor load together with the new beam line SR4b to the east hall. The complete reconstruction allows the incorporation of several improvements.

Neutron beam

The first point to consider in the definition of the neutron beam is to transmit as many cold neutrons as possible from the beam tube's nose to the sample to be irradiated in order to maximize the neutron statistics on the detector. Therefore, the whole channel cross-section 120 mm x 120 mm will be kept open as option for measurements where high flux is required but with relatively low L/D ratio (L/D=166), for example in dynamic measurements. [1] The next option is a small aperture as close as possible to the neutron source to obtain a large fully illuminated area. The best possible position is 4.5 m from the cold source and the aperture is actually a 1 meter long block made of low cobalt steel with a conical channel and a cadmium ring in the smallest opening. This configuration allows a fully illuminated area of 400 mm x 400 mm, L/D=3000 at 20 meters from the cold source and a fully illuminated area of 140 mm x 140 mm, L/D=1500 at 10 meters from the cold source. In order to obtain more options for the beam geometry definition, a drum collimator selector will be integrated into the first shielding block. Within the selector it is possible to fit six collimators with a length of 800 mm. In the first two positions, collimators for L/D=800 and 400 are planned; in the third position one unit with a very narrow aperture (diameter of the aperture of the order of 1 mm) for phase contrast measurements. The fourth position remains fully open with 120 mm x 120 mm. The fifth and sixth are spare positions depending on the future development. An additional option to define the beam geometry is a coded mask positioned directly in the entrance of the first shielding block. It is a cadmium element with numerous pinholes in a non-redundant array pattern. They transmit more neutrons than only one aperture, which reduces the phase contrast exposure time. A consecutive deconvolution of the image must be done by computer [2].

External vertical beam shutter

Outside of the biological shield an external vertical beam shutter will be mounted. This will be the main shutter for ANTARES II as the preceding drum shutter cannot be closed when the beam SR4b is in use. The vertical displacement is simple and allows a simple fail-safe mechanism in case of emergency or power failure [3].

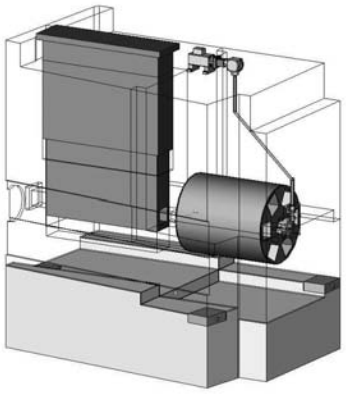

Figure 1: First shielding element with external vertical shutter and drum collimator selector.

Beam formation area

The beam formation area is located in the first chamber directly behind the first shielding element. Here, a group of instruments will be mounted which modify the properties of the neutron beam depending on the requirements of the measurements, including:

Fast shutter: Closes the cold neutron beam between individual images of a tomography and reduces the activation of the sample.

Multi-filter [4]: This is a device for positioning different single crystals in the neutron beam. Sapphire will be used as filter for epithermal neutrons, bismuth and lead as filter for gamma radiation. With a beryllium filter the contrast in neutron radiographies can be increased for combinations of certain materials, as only cold neutrons ($\lambda < 4$Å) are transmitted.

Aperture wheel for phase contrast: A remote controlled wheel for the positioning of cadmium sheets with eight different slotted and circular orifices from 1 mm to 7 mm in diameter.

Double crystal monochromator: Allows energy-dependent measurements between 2.7 Å and 6.5 Å.

Neutron periscope assembly

The first prototypes of neutron periscopes have been designed, built and tested by the ANTARES team at FRM II[5]. Basically, such a periscope consists of a box with two parallel super mirrors. The first mirror reflects neutrons out of the direct line of sight and the second mirror brings the reflected neutrons in a direction parallel to the entrance direction.

The fast and epithermal neutrons and gamma radiation are absorbed in a beam stopper consisting of a block of borated polyethylene and lead. When the periscope is positioned near to the neutron source it is possible to obtain a clean cold neutron beam, and the noise in the measurements is significantly reduced. One disadvantage is the limitation of the field of view due to the small reflection angle (1 to 1.3°) depending of the value m of the mirror. Nevertheless, with a device of about 3 meters length the illuminated field has a width of 100 mm and a height of 50 mm, which is acceptable for most general applications.

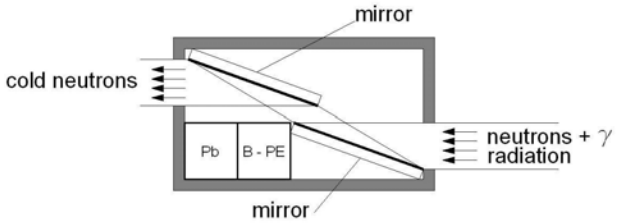

Figure 2: Schematic drawing of neutron periscope.

Flight tube

The new facility ANTARES II will have modular flight tubes adapted to the dimension and position of the neutron beam. The penumbra will be partially absorbed in the partition walls (W1, W2) allowing to reduce the diameter of the flight tubes. The flight tubes are not evacuated. In order to avoid potentially dangerous situations and to reduce the thickness of the entrance and exit windows, the tubes will be filled with He. Because there is no difference in pressure between He inside the flight tubes and the atmosphere outside, the tubes' windows can be made of very thin aluminum sheets.

Shielding

The shielding components are mostly elements with a thickness of 600 mm. They are made of low cobalt steel containers filled with heavy concrete with a density of 4.5to/m^3. The internal side of the walls and the roof is covered with plates of borated polyethylene with a thickness of 50 mm. The thickness of both concrete and polyethylene was optimized with the help of Monte Carlo calculations in order to remain below the allowed radiation dose limit of 5 μSv/h on the outside and to reduce the total weight of the shielding elements. Between the wall elements there are assembly steps avoiding the direct view to the inside through the gap.

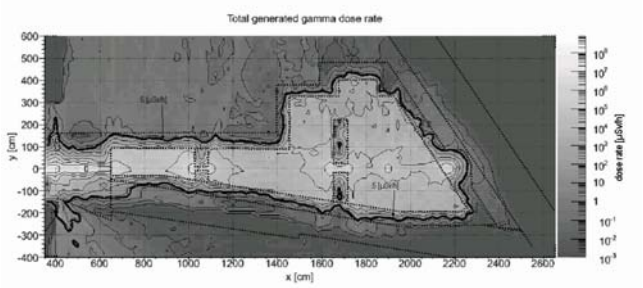

Figure 3: Horizontal cut of ANTARES II with Monte Carlo-simulated gamma radiation dose.

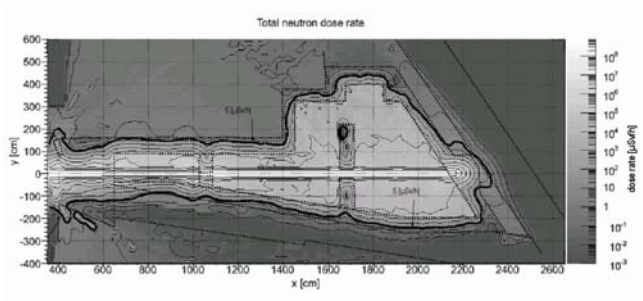

Figure 4: Horizontal cut of ANTARES II with Monte Carlo simulated neutron radiation dose.

Layout of the facility

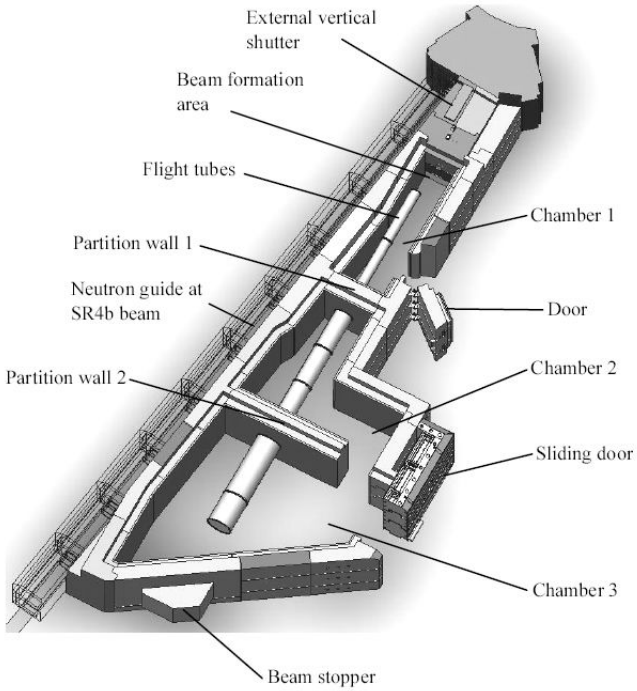

Figure 5: View of ANTARES II with main components.

Outlook

In the beginning of 2010 the new facility ANTARES II should deliver the first images. The new ANTARES II facility will maintain the properties of the first one, while at the same time adding new features and capabilities like special new measurement positions and the possibility to produce a high-resolution and very low background beam with the aid of the neutron periscope; or a very high intensity low-resolution beam for dynamic short-time measurements. The ANTARES II concept remains open and flexible for future additions like a velocity selector or even a chopper for TOF measurements.

References

[1] B. Schillinger, *Nondestr. Test. Eval.*, 16:141-150, 1999.

[2] F. Grünauer, *Nucl. Inst. and Meth. A*, 542:342-352, 2004.

[3] E. Calzada, *Proceedings of the 7th World Conference on Neutron Radiography*, 41-48, 1999.

[4] K. Lorenz, *Proceedings of the 8th World Conference on Neutron Radiography*, 2006.

[5] B. Schillinger, *Nucl. Inst. and Meth. A*, in press.

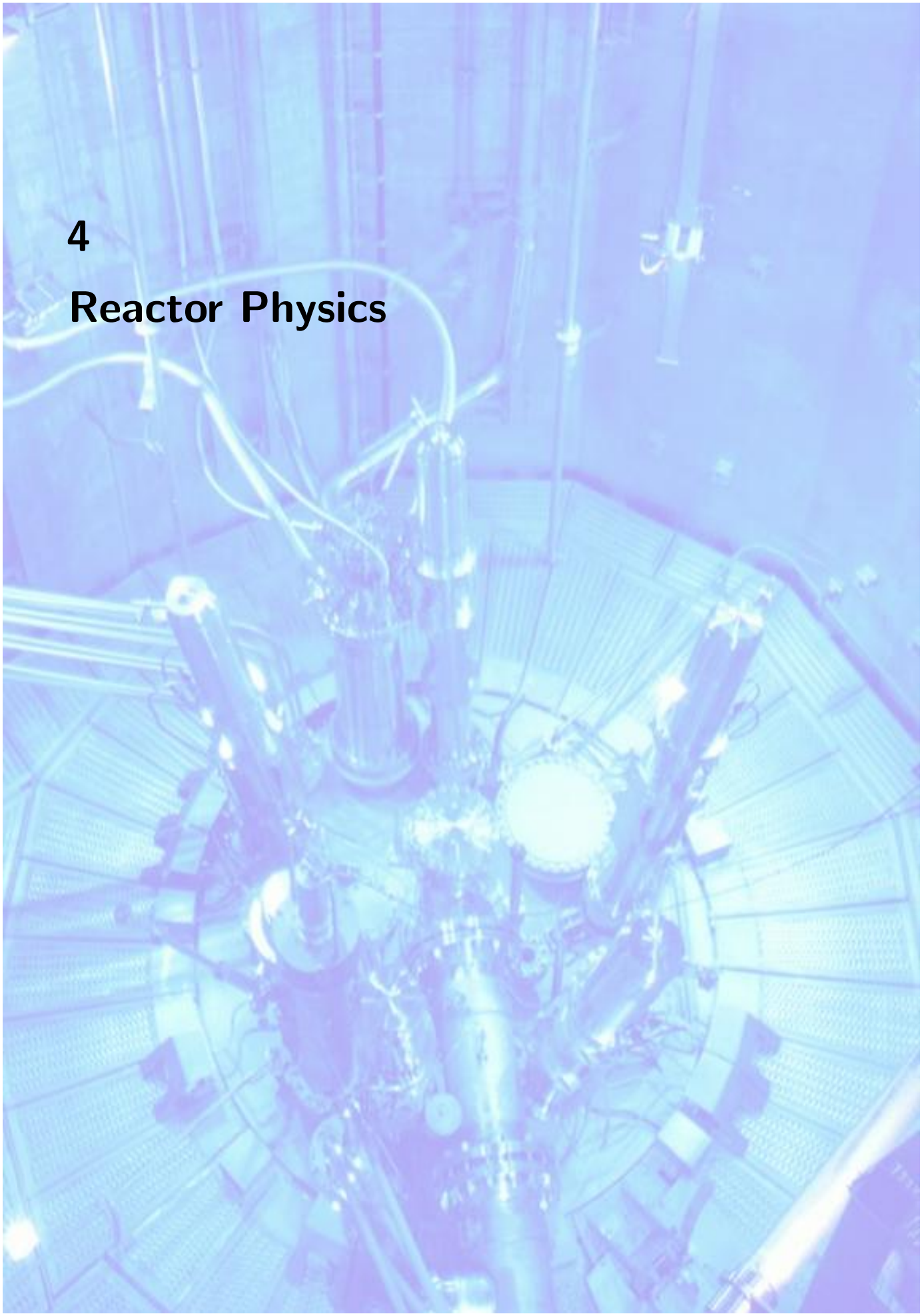

4
Reactor Physics

4.1 Anti Neutrino Spectrum from Fast Neutron Fission of ^{238}U

N. Haag [1], **K. Schreckenbach** [2], **M. Hofmann** [1], **M. Hofmann** [1], **M. Göger-Neff** [1], **L. Oberauer** [1]

[1] *Physik Department E15, Technische Universität München, D-85747 Garching, Germany*
[2] *Physik Department E21, Technische Universität München, D-85747 Garching, Germany*

The antineutrino spectrum from ^{238}U(n$_{fast}$, f) contributes by about 7% to the antineutrino source spectrum of a nuclear power reactor. The precise knowledge of this source spectrum is important for the evaluation of neutrino oscillation experiments carried out at different distances from the reactor (see [1]). We were able to measure this contribution from ^{238}U for the first time using the fast neutron beam at NECTAR at the FRM II. For this purpose a gamma suppressing electron telescope, consisting of a photomultiplier, a plastic scintillator and a multiwire chamber was designed and constructed. Some basic characteristics of the system such as engery calibration, the good energy resolution of the plastic scintillator of 8.5% at 1 MeV and a very high gamma-suppression (better than 99.4%) of the upstream multiwire chamber, could be determined with several radioactive sources. The spectrum was determined relative to the well-known antineutrino spectrum from ^{235}U(n$_{th}$,f) reaction [2], which was also measured with the same detector but the NECTAR beam switched to thermal neutrons. The relative fission events in the two measurements were determined by gamma spectroscopy of the irradiated samples. To determine the antineutrino spectrum of the fission products of ^{238}U the corresponding sum beta spectrum of fission products has to be measured and then converted into the antineutrino spectrum.

Irradiating a natural uranium foil with the thermal neutron beam we could reach a signal-to-background ratio of about 10:1, whereas this ratio at the fast beam was 1:1. Therefore it is a main concern to have an accurate knowledge of the contributing background which was determined by a Pb target. An error in the pulse height recording due to a deficient electronic module limited the energy range to values between 2 to 5 MeV, whereas 2 to 9 MeV where desired. This problem is being solved and will not contribute in a future beam time. The gamma measurements of the irradiated targets – performed by S. Wolff from FRM II radiation safety office – could determine the ratio of fissions in the thermal and the fast beam to 19:1. Furthermore by analyzing gamma rays from fission products with different fission yields in thermal and fast fission, it could be shown, that in the fast beam no significant thermal fission was contributing. Taking into account the background – estimated with the Pb-dummy – we were able to extract the beta spectrum of the fission products of ^{238}U. This could be converted into the antineutrino spectrum (see fig. 1).

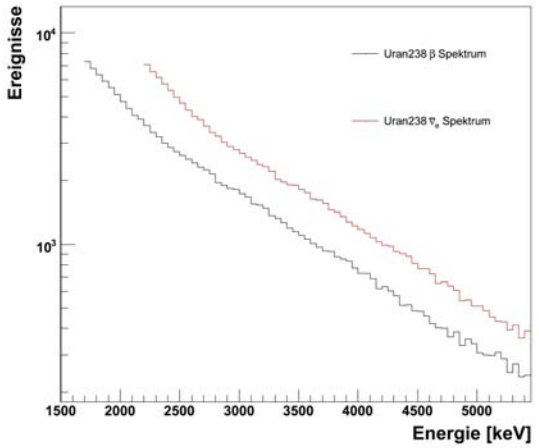

Figure 1: The antineutrino spectrum of the fission products of ^{238}U in logarithmic scale as determined in a first beam time at NECTAR. The bin-width is 50keV.

Acknowledgements:
We like to thank F. M. Wagner and T. Bücherl for their friendly and effective help. We also thank S. Wolff for the time and patience spent with the gamma spectrometry of the irradiated samples, yielding the excellent gamma intensity data.

References

[1] CHOOZ collaboration, *Eur. Phys. J. C*, 27:331, 2003.

[2] K. Schreckenbach et al., *Phys. Lett. B*, 160:325, 1985.

5
Instrument Development

5.1 Cavities with Uniform Ultra-High Polarization

P. Böni [1], **W. Münzer** [1], **A. Ostermann** [2]

[1] *Physik Department E21, Technische Universität München, D-85747 Garching, Germany*

[2] *Forschungsneutronenquelle Heinz Maier-Leibnitz (FRM II), Technische Universität München, D-85747 Garching, Germany*

Neutron scattering with polarization analysis is an indispensable tool for the investigation of novel materials exhibiting electronic, magnetic and orbital degrees of freedom. In addition, polarized neutrons are necessary for neutron spin precession techniques that path the way to obtain extremely high resolution in space and time. Using twin cavities, polarized beams with a homogeneous phase space and $P > 0.99$ can be produced without significantly sacrificing intensity.

In order to improve, we have performed simulations using two V-cavities (Fig. 1) in a crossed and in a parallel geometry following an idea from the ILL, where crossed polarizing benders were combined [1]. The parallel geometry is more convenient because the magnetic field is uniform along the polarizing device and the horizontal and vertical divergence are decoupled. Therefore, coatings with very large m can be used for the top and bottom sides of the cavity. Moreover, there is a freedom for implementing a vertical tapering. We have found that the crossed configuration yields only a marginal 0.2% higher polarization than the parallel configuration.

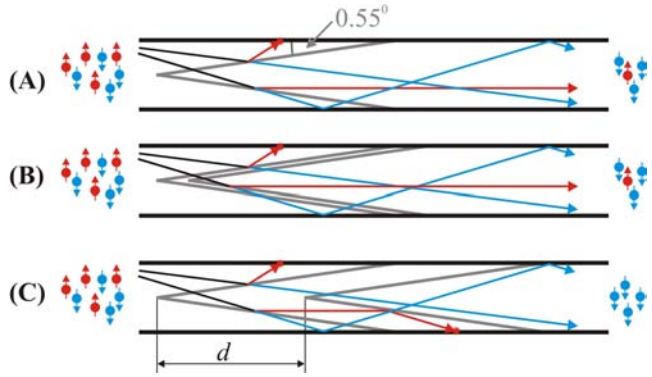

Figure 1: Top view of polarizing cavities. If a single V-cavity is used (A), there is a possibility that neutrons with the up-polarization are transmitted. If the two Vs are displaced by a significant distance d (C), the wrongly polarized neutrons are removed and the polarization of the transmitted beam is increased. If the Vs are too close (B), P does not improve.

To optimize the position of the two Vs we have simulated the polarization of the transmitted neutron beam for various λ and separations d of the polarizing Vs (Fig. 2). The results show that by using a parallel orientation for the Vs, a very high polarization $P > 99\%$ can be achieved for $d > L/2$ and a range of wavelengths 5 Å $< \lambda <$ 18 Å. We assumed that width and coating of the guide are 60 mm and $m = 1.2$, respectively. The taper angle of the cavity was chosen to be 0.55^0 and the polarizing supermirror had a critical angle $m = 3.3$ and $R = 82\%$. The length of the V is $L = 3.125$ m. Note that the Vs are coated on both sides.

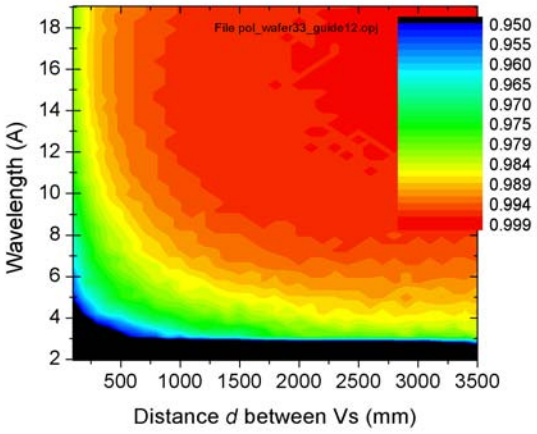

Figure 2: If the separation d of the Vs exceeds $\simeq L/2$, the polarization of the neutrons is above 99% for a large range of λ.

Fig. 3 shows a detailed comparison of the cavities including collimation after polarization. It is seen that the characteristic dip in P near $\lambda = 8$ Å of a single cavity [2], which is most prominent if the divergence of the neutrons is reduced, is strongly reduced for the twin cavity and that the polarization $P > 99\%$ is excellent and only weakly dependent on λ. Therefore, the distortion of the phase space by the two Vs is small, similarly as for ^{3}He polarizers. In contrast for the single cavity, P increases strongly from 87% to 95% near $\lambda = 5$ Å when a 10'collimator is inserted. This effect is particularly disturbing for SANS and reflectometry. Absorption by the additional Si substrates for the Vs can be reduced by using very thin Si wafers.

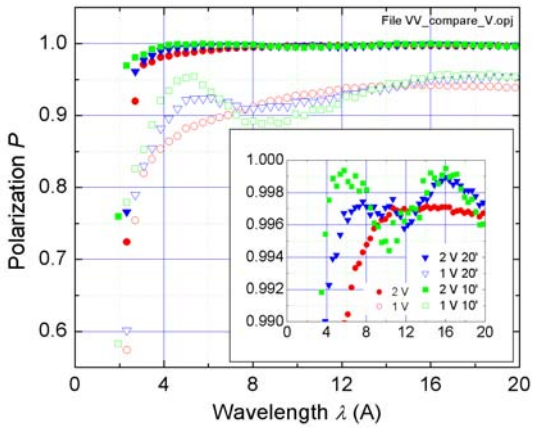

Figure 3: The data shows the polarization of the neutron beam for various collimations after the polarizers: circles: no collimation, triangles: 20', and squares: 10'. The filled and empty symbols show the data for the twin and the single cavity, respectively. The inset shows the high polarization and the excellent uniformity of the twin cavity.

References

[1] M. Kreuz et al., *Nucl. Instr. Meth. A*, 547:583, 2005.

[2] R. Gilles et al., *J. Appl. Cryst.*, 40:428, 2007.

5.2 Focusing Neutrons on Very Tiny Spots

R. Valicu [1, 2], **P. Böni** [1]
[1] *Physik Department E21, Technische Universität München, D-85747 Garching, Germany*
[2] *Forschungsneutronenquelle Heinz Maier-Leibnitz (FRM II), Technische Universität München, D-85747 Garching, Germany*

It is well known that elliptic guides can lead to significant gains in flux [1] and improve the resolution of beam lines for neutron scattering [2]. Moreover, the phase space of the transmitted neutrons is more homogeneous and the focusing at the sample position can be improved. The focusing guide that was installed at the beam line PGAA at FRM II is composed of 2 elliptical focusing neutron guides with supermirror (SM) coating $m = 3$. The first and second guide has a length of 5.8 m and 1.09 m, respectively and are separated by a thin aluminum window. This configuration has the performance as given in Table 1. Fig. 1 shows the intensity distribution in the focal point of the second elliptic guide.

Position	neutron flux ($cm^{-2}s^{-1}$)	beam profile $h \times w$ (mm^2)	remarks
end of guide	$6.0 \cdot 10^9$	28×62	measured
after first elliptic guide	$7.3 \cdot 10^9$	14×38	calculated
after second elliptic guide	$20 \cdot 10^9$	4×11	calculated

Table 1: Performance of the existing guide of PGAA beam line at FRM II

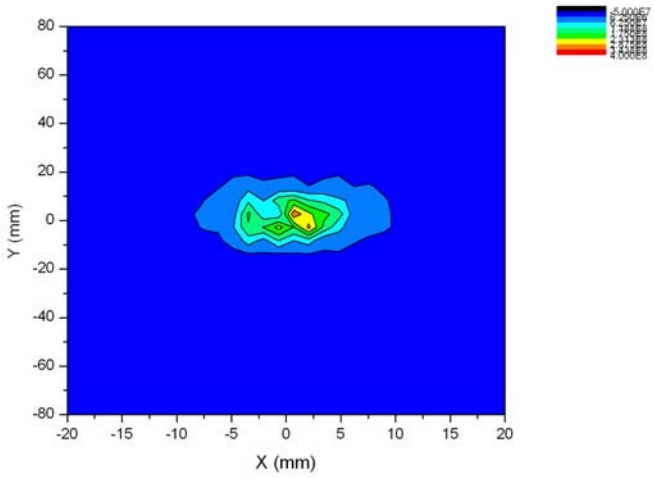

Figure 1: Neutron flux in the focal point of the existing elliptic guide 2.

In order to improve the spatial focusing of the neutron beam we have designed a third elliptic neutron guide that may be added after the second elliptic guide. In a first step, we have assumed that the length of the third guide is 75 mm. Using the Monte-Carlo simulation tool McStas we have simulated the performance using supermirror coatings with $m = 5$ and $m = 6$. We considered a wavelength band 1 Å $< \lambda <$ 21 Å and a neutron flux $f = 10^{10}$ $cm^{-2}s^{-1}$.

Fig. 2 demonstrates that the beam size can be significantly reduced when a third elliptic guide with supermirror $m = 5$ is added. Moreover, the neutron flux is increased. Using coatings with $m = 6$ is even more efficient because neutrons with smaller λ are also transmitted by the guide (Fig. 3).

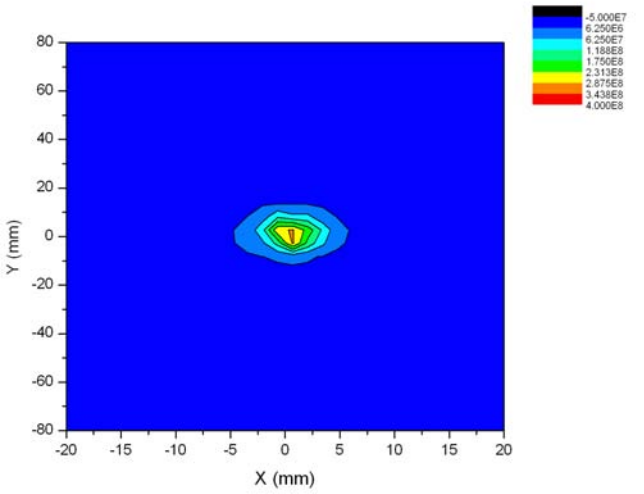

Figure 2: Neutron flux in the focal point of the third elliptic guide with $m = 5$.

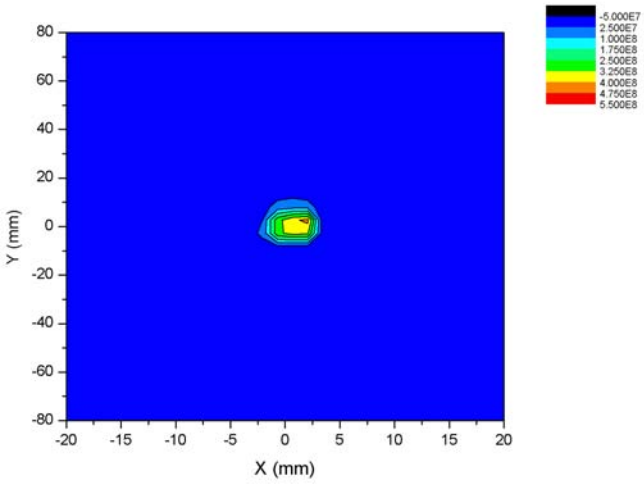

Figure 3: Neutron flux in the focal point of the third elliptic guide with $m = 6$.

We have also calculated the flux-gain by dividing the intensity averaged over a central area of 4 mm $\times$1 mm of the position sensitive detector in the focal point after adding the third elliptic guide (Table 2). It is seen that a gain of at least a factor of 2 can be achieved.

Item	initial position	SM with $m = 5$	SM with $m = 6$
flux ($cm^{-2}s^{-1}$)	$14 \cdot 10^9$	$35 \cdot 10^9$	$39 \cdot 10^9$
gain in flux	1	2.5	2.8

Table 2: Gain as obtained after adding a third elliptic guide

The next step was to vary the length of the third guide in the range 40 mm $< L <$ 90 mm to find the optimum providing the largest gain. It became clear that $L = 80$ mm yields the largest gain, i.e. $G = 3.1$. The third guide produces a focal spot with the dimension 4 mm $\times$ 9 mm.

Finally, we inserted an aperture between the exit of the guide and the sample position in order to reduce the dimension of the neutron spot at the focal position significantly. Table 3 gives a summary of the beam diameter and the respective flux vs. the diameter of the aperture.

Diam. of aperture (mm)	flux at focal point ($cm^{-2}s^{-1}$)	beam diameter (μm)
0.2	$0.8 \cdot 10^9$	36
0.4	$1.9 \cdot 10^9$	120
0.6	$1.6 \cdot 10^9$	160
0.8	$1.5 \cdot 10^9$	180
1.0	$1.6 \cdot 10^9$	200

Table 3: Profile of neutron beam at the focal point after the introduction of an aperture

The results show that it is possible to reduce the diameter of the focused beam to a diameter as small as 35 μm while maintaining a reasonably high flux of approximately 10^9 neutrons per cm^2 and s.

References

[1] C. Schanzer et al., *Nucl. Instr. Meth. A*, 529:63, 2004.

[2] P. Böni, *Nucl. Instr. Meth. A*, 586:1 2008.

5.3 Diffractometer MIRA at FRM II

R. Georgii [1, 2], **P. Böni** [1], **R. Schwikowski** [1, 2]
[1] *Physik Department E21, Technische Universität München, D-85747 Garching, Germany*
[2] *Forschungsneutronenquelle Heinz Maier-Leibnitz (FRM II), Technische Universität München, D-85747 Garching, Germany*

MIRA at FRM-II is a versatile instrument for very cold neutrons (VCN) using neutrons with a wavelength $\lambda > 8$ Å. The flux at the sample position is $5 \cdot 10^5$ neutrons/(cm^2 s) unpolarised. It is situated at the cold neutron guide NL6b in the neutron guide hall of the FRM-II. As the instrument set-up can be changed quickly, MIRA is ideally suited as a testing platform for realizing new instrumental set-ups and ideas. In particular, MIRA is unique in its possibilities of combining different neutron scattering methods as:

- Polarized or non-polarized reflectometry
- Spherical polarimetry
- Polarized or non-polarized small angle scattering (SANS)
- Classical NRSE (Neutron Resonance Spin Echo) setup using the MIEZE principle

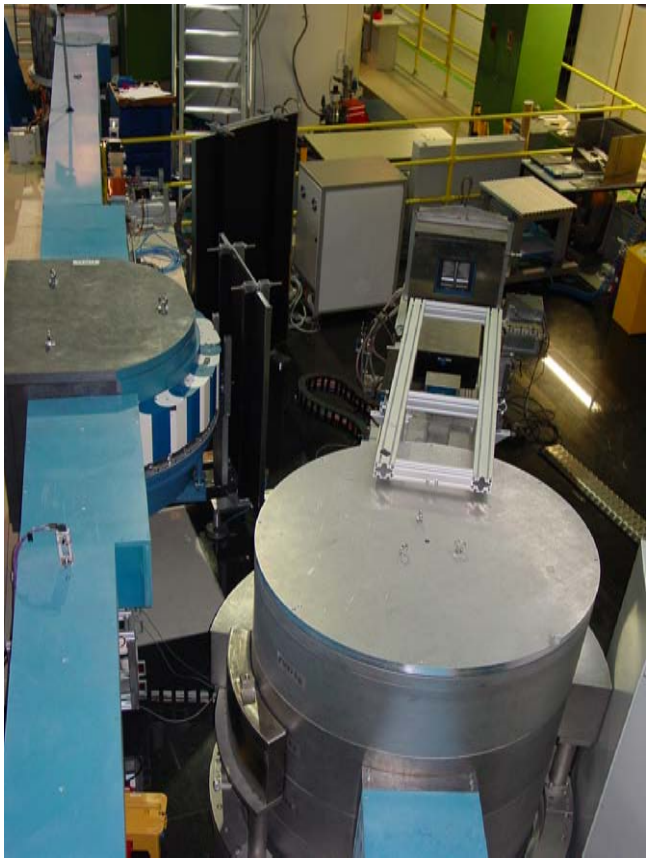

Figure 1: The two beam ports for MIRA. Left the port for wavelengths between 3 Å and 6 Å. Right the old beam port for wavelengths above 8 Å.

In 2008 MIRA was operating successfully for 4 cycles of the FRM-II, in total 240 days. A total number of 11 user-experiments, 12 internal experiments, together with extensive tests and service measurements were performed. A total of 2 weeks was devoted to the Fortgeschrittenenpraktikum of the Physik Department for 24 students in total. The main part of the beam time was devoted to SANS measurements in helical magnets (see 1.1) and the development of MIEZE. In total 6 publications were published this year, one of them in Science. One student (Leo Polz) from the Fachhochschule München spent his practical semester at MIRA constructing and building the motorization of our magnet. A physics student in his 5th year from the TU Delft (Jörgen Konings) passes currently his practical training semester at MIRA performing Monte Carlo simulations of the MIEZE setup.

Currently the upgrade of MIRA to shorter wavelengths is in progress. The goal is to use neutrons with wavelengths between 3 Å and 6 Å from the neutron guide NL 6a (beam area 120 x 60 mm^2) using a PG monochromator (see Figure 1). The polygraphite (PG) monochromator and its mechanics (see Figure 2) have been installed and first tests at 4.3 Å yield at the sample position a flux of $3 \cdot 10^6$ neutrons/(cm^2 s) unpolarised for a fixed focusation of the PG monochromator.

Figure 2: The PG monochromator with its electronics.

5.4 RESEDA in Operation

W. Häußler [1, 2], **J. Kindervater** [2], **M. Sandhofer** [1], **R. Schwikowski** [2], **A. Mantwill** [1], **P. Böni** [1]
[1] *Physik Department E21, Technische Universität München, D-85747 Garching, Germany*
[2] *Forschungsneutronenquelle Heinz Maier-Leibnitz (FRM II), Technische Universität München, D-85747 Garching, Germany*

At RESEDA in 2008, first Neutron Spin Echo (NSE) and Neutron Resonance Spin Echo (NRSE) experiments have been performed. Critical dynamics in a magnetic system and dynamics in a metal melt have been studied, and a challenging new NRSE technique for detection of neutron polarization oscillating with high frequency has been tested at RESEDA in collaboration with a group of scientists from the University of Heidelberg. During these first experimental studies, the neutron velocity selector had to be demounted and sent away for maintenance works. Exchanging the selector, and reinstallation have been accomplished within only two days for each task - thanks to the good collaboration of several groups providing technical support at FRM II.

Before these first experiments, the commissioning phase of the instrument had taken place, during the first months of 2008, including demagnetization of the mu-metal shielding, revision of the coupling coils and the fine-tuning of the RF circuits. Having finished preliminary polarization measurements, the NRSE coils have been put into operation and we started then with spin echo test measurements, employing NRSE together with NSE, the latter by using solenoids for measurements at small spin echo times. Moreover, an improved design of the radiation shielding covering the new polarizer, shutter, attenuators and beam monitor at the primary side of the spectrometer has been constructed, and will be installed as soon as it is delivered.

Further NSE and NRSE experiments proposed by scientists from Germany, England and Switzerland have taken place in the meantime at RESEDA.

After having commissioned the instrument as described above, and during ongoing experiments are performed, the instrument is still being improved step by step. The NRSE coils suffering from corrosion due to the mixture of copper and aluminium parts are being repaired. Additional NRSE coils are going to be built, in order to make and keep RESEDA fully operational. RESEDA is operational with one primary and one secondary spectrometer arm. A special feature of the NRSE method will be used soon: NRSE allows in a straightforward way for installing additional secondary spectrometer arms. The secondary spectrometer of RESEDA is being doubled at the moment: the installation of the spin echo coils used for measurements at small spin echo times, and of the analyser/detection system has started already, in order to be able to simultaneously operate two secondary spectrometer arms. In addition, two of the NRSE coils being under construction at the moment, will be installed and put into operation in this supplementary spectrometer arm. In 2009, after having finished these installations, RESEDA will be operational with doubled solid angle for neutron detection.

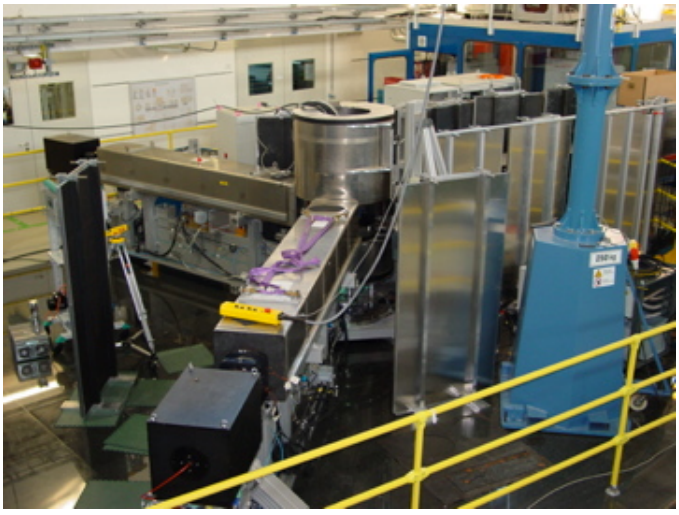

Figure 1: RESEDA with primary (left) and two secondary spectrometer arms, one of them being in operation, the other one in commissioning.

5.5 Transmission Measurements of UCN Guides by UCN Capture Activation Analysis of Vanadium

K. Schreckenbach [1], **A. Frei** [2], **J. Hartmann** [2], **B. Franke** [2], **T. Huber** [2], **R. Picker** [2], **S. Paul** [2], **P. Geltenbort** [3]

[1] *Physik Department E21, Technische Universität München, D-85747 Garching, Germany*
[2] *Physik Department E18, Technische Universität München, D-85747 Garching, Germany*
[3] *Institut Laue Langevin, 38042 Grenoble, France*

The transport of ultra cold neutrons (UCN) in guides from the source to the experimental site is a major issue for various kinds of precision experiments, as for the planned UCN beam port at the FRM II at a distance of 40 m from the source. We have developed a novel method for UCN transmission measurement. At the PN2 TES beam at the ILL the UCN were absorbed at the end of the guide in a vanadium plate. At a vanadium surface UCN reflection is small due to the Fermi potential of -7 neV [1]. The UCN absorption produces a beta unstable nucleus $^{5}2$V with a half live of 3.74 min and a 1434 keV gamma ray following the beta decay. It was measured by a NaI detector system. UCN guides (diameter: 66 mm) of the repliqua type from PNPI and from Heidelberg were investigated and the UCN loss per meter was measured by varying the guide length. By an absolute calibration of the gamma detection system we deduced also the absolute value of the UCN current absorbed in the vanadium plate.

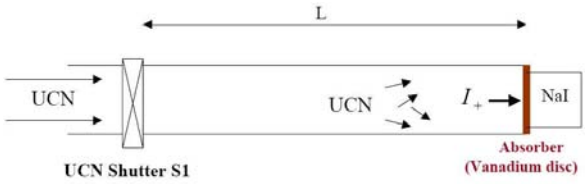

Figure 1: Scheme of the UCN current measurement for the determination of the transmission of UCN guides of length L. The UCN beam spectrum was shaped before entering the beam line. The UCN current I_+ is absorbed in the Vanadium disc.

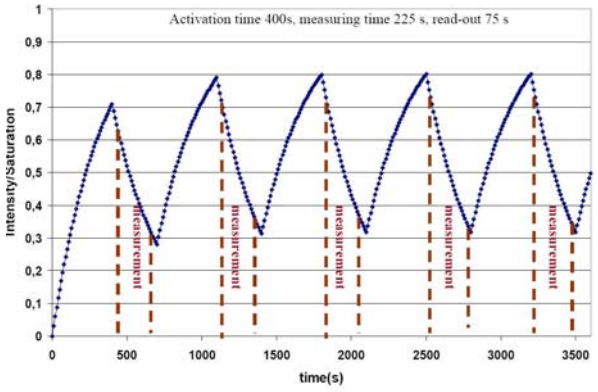

Figure 2: Alternate activation and decay measurement with the vanadium UCN beam absorber. The number of ^{52}V is given in units of saturation. The time slabs for the measurement of the 1434 keV gamma line are indicated.

Fig. 2 shows schematically the built up of the activity in the vanadium disc. For the background measurement the valve S1 was kept closed. The result for the transmission was 95.6 ± 0.6 % per m for the PNPI guide and 95.9 ± 0.6 % per m for the Heidelberg guide, but the guides were not gap free. The NaI detector set-up yields 4.7(2)% efficiency as calibrated later at the FRM II in a comparative measurement with an HPGe detector of the health physics group.

In conclusion we have developed a technique for measuring reliably the UCN current at the end of an UCN guide and have determined the transmission of repliqua type UCN guides. For a guide of a diameter as planned for the FRM II UCN line (120-160 mm diameter) and avoiding UCN leakages from gaps, a transmission for a 40 m guide of better than 50% may be achieved. The presented activation method is well suited for a limited application of UCN detection cases, where an accumulated detection of the UCN ensemble is adequate.

Acknowledgement: The authors acknowledge the technical support by the ILL. We are thankful to S. Wolff from the FRM II health physics group for the comparative HPGe measurements in the absolute calibration of the NaI detector. The research is supported by the DFG cluster of excellence *Origin and structure of the universe*.

References

[1] K. Schreckenbach et al., *Phys. Lett. B*, 160:325, 1985.

6

Activities 2008

6.1 Lectures, Courses and Seminars

A. Bauer	Tutor "Mathematische Methoden der Chemie I" (WS 07/08) Tutor "Mathematische Methoden der Chemie II" (SS 08)
P. Böni	Lecture "Experimentalphysik I für Geodäsie und Geoinformation" (WS 2007/08) Tutorials "Experimentalphysik I für Geodäsie und Geoinformation" (WS 2007/08) Lecture "Experimentalphysik II für Geodäsie und Geoinformation" (SS 08) Tutorials "Experimentalphysik II für Geodäsie und Geoinformation" (SS 08) Lectures "Neutron Scattering and Phase Transitons", Joint Swedish-German Summer School, Nässlingen, Sweden, Sep. 15-19, 2008 Seminar "Neutronen in Industrie und Forschung" , together with W. Petry, K. Schreckenbach and W. Häußler Seminar "Experimentelle Methoden in der Festkörperphysik" together with C. Pfleiderer and C. Hugenschmidt
R. Georgii	Lab course "Fortgeschrittenenpraktikum für Physiker" (at FRM II)
W. Häußler	Seminar "Neutronen in Forschung und Industrie" together with P. Böni, W. Petry and K. Schreckenbach
C. Hugenschmidt	Lecture "Physik mit Positronen I" (SS 08) Seminar "Experimentelle Methoden der Festköperphysik", together with C. Pfleiderer and P. Böni Lab course "F-Praktikum Positronen-Annihilation"
M. Janoschek	Tutor "Experimentalphysik I für Geodäsie und Geoinformation" (WS 07/08) Tutor "Experimentalphysik II für Geodäsie und Geoinformation" (SS 08)
F. Jonietz	Tutor "Experimentalphysik II" (SS 08)
T. Keller	Lab course "Elektronikpraktikum"
S. Legl	Tutor "Experimentalphysik I" (WS 07/08)
J. Mayer	Tutor "Experimentalphysik I" (WS 07/08) Tutor "Experimentalphysik II" (SS 08)
C. Morkel	Lecture "Physics with Neutrons I" (WS 07/08) Lecture "Physics with Neutrons II" (SS 08)
M. Mühlbauer	Lab course "Elektronikpraktikum" Tutor "Experimentalphysik I für Geodäsie und Geoinformation" (WS 2007/08)
S. Mühlbauer	Tutor "Experimentalphysik I" (WS 07/08)
A. Neubauer	Tutor "Experimentalphysik I" (WS 07/08)

P. Pikart	Lab course "F-Praktikum Positronen-Annihilation"
C. Pfleiderer	Lecture "Experimentalphysik I" (WS 07/08)
	Tutorials "Experimentalphysik I"
	Lecture "Experimentalphysik II" (SS 08)
	Tutorials "Experimentalphysik II"
	Seminar "Experimentelle Methoden der Festköperphysik", together with P. Böni and C. Hugenschmidt
	Seminar "Makroskopische Quantenphänomene", together with R. Gross, R. Hackl, S. Gönnenwein and S. Dunsiger (SS 08)
	"Münchner Physik Kolloquium", Coordinator (TUM)
C. Piochacz	Tutor "Experimentalphysik I" (WS 07/08)
	Lab course "F-Praktikum Positronen-Annihilation"
R. Ritz	Tutor "Experimentalphysik II" (SS 08)
M. Schulz	Lab course "Elektronikpraktikum"
B. Schillinger	Lab course "Elektronikpraktikum"
K. Schreckenbach	Lecture "Reaktorphysik und neue Methoden der Kerntechnik"
	Seminar "Neutronen in Forschung und Industrie", together with P. Böni, W. Petry and W. Häußler
	Lab course "Fortgeschrittenenpraktikum für Physiker" (at FRM II)

6.2 Seminar "Neutronen in Industrie und Forschung" 2008

Date	Speaker	Title
Jan 7	K. Kirch	Ultracold neutron physics – an update from PSI
Jan 14	T. Weber	Modeling quasicrystals - modeling complexity
Jan 28	C. Kraemer	Quantum phase transition of a magnet in a spinbath
Feb 18	J. Schneider	TOF-Instrumente mit statistischen Choppern
Apr 21	A. Senyshyn	SPODI
Apr 28	H. Abele	The neutron alphabet
May 5	P. Link	Magnetic properties of R_2PdSi_3 (R = Rare Earth) studied with elastic and inelastic neutron scattering
May 19	A. Krimmel	Neutron scattering studies of exotic magnetic ground states in spinel compounds
May 23	P. Fierlinger	Messung des elektrischen Dipolmoments des Neutrons
Jun 6	V. Hutanu	POLI-HEiDi, the new polarised neutron diffractometer at hot source SR9 - advances and perspectives
Jun 9	R. Hermann	Lattice dynamics in emerging functional materials
Jun 16	K. Schreckenbach	Generation IV Reaktoren
Jun 24	C. Hugenschmidt	Von der Oberfläche ins Volumen – niederenergetische Positronen als Sonden im Festkörper
Jun 30	S. Mühlbauer	Vortex lattices in superconductors – Measured with small angle neutron scattering
Jul 7	A. S. Wills	Some structures in magnetism
Jul 14	A. Rühm	The neutron/X-ray contrast and spin-echo reflectometer N-REX+ at FRM-II: present status and future perspectives
Aug 4	P. Fierlinger	The search for particle electric dipole moments
Oct 14	M. K. Sanyal	Polarized neutron refelectivity study of two-dimensional spin ordering in Gadolinium Stearate Lb films at milli-Kelvin temperatures
Oct 20	M. Schreck	Large-area diamond mosaic crystals from the gas phase
Oct 27	S. Klimko	NRSE on IN22 at the ILL - development, realization and first applications
Nov 10	H. Boysen	Investigating solid ionic conductors by neutron powder diffraction
Nov 17	C. Pappas	How much larmor precession affords chirality ?
Nov 24	W. Doster	A neutron scattering view of protein dynamics
Dec 1	M. Schulz	Radiography with polarized neutrons
Dec 8	S. Studeny	Development of a biophysical treatment planning system for the FRM II neutron therapy beamline
Dec 15	A. K. Freund	Optimisation and fabrication of composite focusing pyrolytic graphite monochromators
Dec 16	M. Sharp	Using SANS to study the solubilisation of model adjuvants by Pluronic block copolymers

6.3 Publications 2008

[1] M. Ay, J. Stahn, and P. Böni. Proceedings of the European workshop on neutron optics NOP'07. *Nucl. Instr. and Meth. A*, 586, 2008.

[2] FJ Bermejo, C. Cabrillo, E. Bychkov, and et al. Tracking the effects of rigidity percolation down to the liquid state: Relaxational dynamics of binary chalcogen melts. *Phys. Rev. Lett.*, 100:245902, 2008.

[3] P. Böni. New concepts for neutron instrumentation. *Nucl. Instr. and Meth. A*, 586:1–8, 2008.

[4] S. R. Dunsiger, Y. Zhao, B. D. Gaulin, Y. Qiu, P. Bourges, Y. Sidis, J. R. D. Copley, A. Kallin, E. M. Mazurek, and H. A. Dabkowska. Diagonal and collinear incommensurate spin structures in underdoped $La_{2-x}Ba_xCuO_4$. *Phys. Rev. B*, 78:092507, 2008.

[5] S. R. Dunsiger, Y. Zhao, Z. Yamani, W. J. L. Buyers, H. Dabkowska, and B. D. Gaulin. Incommensurate spin ordering and fluctuations in underdoped $La_{2-x}Ba_xCuO_4$. *Phys. Rev. B*, 77:224410, 2008.

[6] R. Gebhard, B. Haas-Gebhard, C. Thomas, E. Calzada, M. Mühlbauer, and B. Schillinger. Untersuchung einer frühmittelalterlichen Spathascheide mit Neutronentomographie. *Restaurierung und Archäologie*, in print.

[7] W. Häußler. Neutron spin echo studies on ferritin: Free-particle diffusion and interacting solutions. *European Biophysics Journal*, 37:563–571, 2008.

[8] W. Häußler, D. Streibl, and P. Böni. RESEDA: double and multi-detector arms for neutron resonance spin echo spectrometers. *Measurement Science and Technology*, 19:034015, 2008.

[9] C. Hugenschmidt, T. Brunner, J. Mayer, C. Piochacz, K. Schreckenbach, and M. Stadlbauer. Determination of positron beam parameters by various diagnostic techniques. *Appl. Surf. Sci.*, 255:50–53, 2008.

[10] C. Hugenschmidt, G. Dollinger, W. Egger, G. Kögel, B. Löwe, J. Mayer, P. Pikart, C. Piochacz, R. Repper, K. Schreckenbach, P. Sperr, and M. Stadlbauer. Surface and bulk investigations at the high intensity positron beam facility NEPOMUC. *Appl. Surf. Sci.*, 255:29–32, 2008.

[11] C. Hugenschmidt, B. Löwe, J. Mayer, C. Piochacz, P. Pikart, R. Repper, M. Stadlbauer, and K. Schreckenbach. Unprecedented intensity of a low-energy positron beam. *Nuclear Instruments and Methods in Physics Research Section A: Accelerators, Spectrometers, Detectors and Associated Equipment*, 593:616–618, 2008.

[12] C. Hugenschmidt, P. Pikart, M. Stadlbauer, and K. Schreckenbach. High elemental selectivity to Sn submonolayers embedded in Al using positron annihilation spectroscopy. *Phys. Rev. B (Condensed Matter and Materials Physics)*, 77:092105, 2008.

[13] A. Ioffe, V. Bodnarchuk, K. Bussmann, R. Müller, and R. Georgii. A new neutron spin-echo spectrometer with time-gradient magnetic fields: First experimental test. *NIM A*, 586:36–40, 2008.

[14] S. Mühlbauer, P. Böni, R. Georgii, A. Schmehl, D. G. Schlom, and J. Mannhart. Field and temperature dependence of the magnetization in ferromagnetic EuO thin films. *Phys.: Condens. Matter*, 20:104230, 2008.

[15] S. Mühlbauer, P.G. Niklowitz, M. Stadlbauer, R. Georgii, P. Link, J. Stahn, and P. Böni. Elliptic neutron guides – focusing on tiny samples. *Nucl. Instrum. Meth. A*, 586:77, 2008.

[16] H. Nozaki, J. Sugiyama, M. Janoschek, B. Roessli, V. Pomjakushin, L. Keller, H. Yoshida, and Z. Hiroi. Neutron diffraction study on two-dimensional Ni oxides; Ag_2NiO_2. *J. Phys.: Condens. Matter*, 20:104236, 2008.

[17] S. R. Parnell, E. Babcock, K. Nünighoff, M. W. A. Skoda, S. Boag, S. Masalovich, R. Georgii, and J. M. Wild. Neutron polarimetry of highly polarised ^{3}He. *NIM A*, http://dx.doi.org/10.1016/j.nima.2008.10.009, 2008.

[18] J. Perlich, V. Körstgens, E. Metwalli, L. Schulz, R. Georgii, and P. Müller-Buschbaum. Solvent content in thin spin-coated polystyrene homopolymer films. *Macromolecules*, http://pubs.acs.org/doi/pdf/10.1021/ma801878j, 2008.

[19] C. Pfleiderer. Borderline metals (news and views). *Nature*, 455:1188, 2008.

[20] B. Roessli, P. Fischer, P. J. Brown, M. Janoschek, D. Sheptyakov, S. N. Gvasaliya, B. Ouladdiaf, O. Zaharko, E. Golovenchits, and V. Sanina. Noncentrosymmetric commensurate magnetic ordering of multiferroic $ErMn_2O_5$. *J. Phys.: Condens. Matter*, 20:485216, 2008.

[21] P. Sperr, W. Egger, G. Kögel, G. Dollinger, C. Hugenschmidt, R. Repper, and C. Piochacz. Status of the pulsed low energy positron beam system (PLEPS) at the Munich research reactor FRM II. *Appl. Surf. Sci.*, 255:35–38, 2008.

[22] M. Stadlbauer, C. Hugenschmidt, and K. Schreckenbach. New design of the CDB-spectrometer at NEPOMUC for T-dependent defect spectroscopy in Mg. *Appl. Surf. Sci.*, 255:136–138, 2008.

[23] SCM Teixeira, G. Zaccai, J. Ankner, and et al. New sources and instrumentation for neutrons in biology. *Chemical Physics*, 345:133–151, 2008.

[24] N. V. Volkov, K. A. Sablina, E. V. Eremin, P. Böni, V. R. Shah, I. N. Flerov, A. Kartashev, J. C. E. Rasch, M. Boehm, and J. Schefer. Heat capacity of a mixed-valence manganese oxide $Pb_3Mn_7O_{15}$. *J. Phys.: Condens. Matter*, 20:445214, 2008.

[25] U. Wasmuth, L. Meier, M. Hofmann, M. Mühlbauer, V. Stege, and H. Hoffmann. Optimisation of composite castings by means of neutron measurements. *CIRP Annals - Manufacturing Technology*, 57:579–582, 2008.

[26] K. Wood, C. Caronna, P. Flouquet, and et al. A benchmark for protein dynamics: Ribonuclease a measured by neutron scattering in a large wavevector-energy transfer range. *Chemical physics*, 345:305–314, 2008.

6.4 Conference, Workshop and Seminar Contributions 2008

[1] P. Böni. Instrumentation with polarized neutrons. Invited Talk. *Workshop on Polarized Neutrons in Condensed Matter Investigations PNCMI 2008, October 2008. Tokai, Japan.*

[2] P. Böni. Introduction to neutron scattering. Invited Talk. *Frontiers in Modern Magnetism - Magnetic Phase Transitions, A Joint Swedish-German Summer School, September 2008. Nässlingen, Sweden.*

[3] P. Böni. Magnetismus aus der Sicht der Neutronen. Invited Talk. *Edgar-Lüscher Lectures, Akademie für Lehrerfortbildung, September 2008. Dillingen, Germany.*

[4] P. Böni. Neutron scattering and phase transitons. Invited Talk. *Frontiers in Modern Magnetism - Magnetic Phase Transitions, A Joint Swedish-German Summer School, September 2008. Nässlingen, Sweden.*

[5] E. Calzada, F. Grünauer, M. Mühlbauer, B. Schillinger, and M. Schulz. New design for the ANTARES-II facility for neutron imaging at FRM II. Talk. *International Topical Meeting on Neutron Radiography, September 2008. Kobe, Japan.*

[6] S.R. Dunsiger, J.P. Carlo, T. Goko, G. Nieuwenhuys, T. Prokscha, E. Morenzoni, D. Chiba, T. Tanikawa, F. Matsukura, H. Ohno, R.H. Heffner, and Y.J. Uemura. Low-energy μSR and transport studies of the doped magnetic semiconductor (Ga,Mn)As. Talk. *11th International Conference on Muon Spin Rotation, Relaxation and Resonance, July 2008. Tsukuba, Japan.*

[7] S.R. Dunsiger, R.F. Kiefl, S.T. Bramwell, K.H. Chow, J.P. Clancy, J.R.D. Copley, H.A. Dabkowska, J.S. Gardner, B.D. Gaulin, J. Lago, R.I. Miller, G.D. Morris, A.N. Price, Y. Qiu, J.P. Ruff, and J.E. Sonier. Spin dynamics of frozen spin ice. Poster. *Highly Frustrated Magnetism 2008, September 2008.*

[8] R. Georgii. MIEZE: First results and perspectives. Talk. *JCNS Workshop, September 2008. Bernried, Germany.*

[9] W. Häußler. Comparison of diffusive dynamics in different protein solutions. Invited Talk. *Meeting of the Soft Matter Group of the University of Tübingen, March 2008. Tübingen, Germany.*

[10] W. Häußler. Neutron spin echo on Apoferritin in solution: The time scale of diffusion. Invited Talk. *Seminar talk College 8 at the Institut Laue-Langevin, October 2008. Grenoble, France.*

[11] W. Häußler and B. Gohla-Neudecker. Differences of diffusive dynamics in solutions of globular proteins. Poster. *Conference on Liquid Matter, June 2008. Lund, Sweden.*

[12] W. Häußler and B. Gohla-Neudecker. NSE studies on diffusive dynamics in Ferritin solutions. Talk. *Workshop on Biomolecular Dynamics and Protein-Water Interactions, September 2008. Feldafing, Germany.*

[13] W. Häußler, A. Ostermann, and P. Böni. The new polarizer at RESEDA - simulation and first experimental results. Poster. *Deutsche Neutronenstreutagung, September 2008. Garching, Germany.*

[14] W. Häussler and B. Gohla-Neudecker. Q-dependence of diffusive dynamics in solutions of globular proteins studied by neutron spin echo. Talk. *Conference on Biological Physics at Large Scale Facilities, October 2008. Grenoble, France.*

[15] C. Hugenschmidt. Surface and bulk investigations at the high intensity positron beam facility NEPOMUC. Invited Talk. *DPG Frühjahrstagung, February 2008. Berlin, Germany.*

[16] M. Janoschek. Search for helimagnon excitations in MnSi: an inelastic neutron scattering study. Poster. *Deutsche Neutronenstreutagung, Technische Universität München, September 2008. Garching, Germany.*

[17] M. Janoschek. Spherical neutron polarimetry of the magnetic structure in MnSi. Talk. *72. Jahrestagung der DPG at TU Berlin, February 2008. Berlin, Germany.*

[18] M. Janoschek. The chiral magnets MnSi and $NdFe_3(^{11}BO_3)_4$ investigated by means of neutron scattering. Talk. *Seminar of the II. Physikalisches Institut at Universität zu Köln, July 2008. Cologne, Germany.*

[19] M. Janoschek. The magnetic structure of $NdFe_3(^{11}BO_3)_4$ investigated by spherical neutron polarimetry. Talk. *Annual Meeting of the SPS , April 2008. Geneva, Switzerland.*

[20] S. Legl. Magnetisation and magnetotransport of ferromagnetic Pr_5Si_3 under pressure. Talk. *Conference on Strongly Correlated Electron Systems, August 2008. Buzios, Brasil.*

[21] J. Mayer, K. Schreckenbach, and C. Hugenschmidt. PAES - Positron annihilation induced Auger electron spectroscopy. Poster. *DPG Frühjahrstagung, February 2008. Berlin, Germany.*

[22] S. Mühlbauer. Intrinsic bulk vortex dynamics revealed by time resolved small angle neutron scattering. Poster. *Conference on Strongly Correlated Electron Systems, August 2008. Buzios, Brasil.*

[23] S. Mühlbauer. Preparation of short neutron pulses using the multi-level MIEZE principle. Talk. *Seminar: Neutrons in Science and Industry, Technische Universität München, June 2008. Garching, Germany.*

[24] S. Mühlbauer. Vortex lattices in superconductors - measured with small angle neutron scattering: Time resolved stroboscopic SANS on niobium, symmetry breaking vortex structures in niobium. Talk. *DPG Frühjahrstagung, February 2008. Berlin, Germany.*

[25] A. Neubauer. Neutron depolarisation measurements on Fe_2TiSn and Ni_3Al. Talk. *Workshop der DGKK, September 2008. Frankfurt, Germany.*

[26] A. Neubauer. Optical-image-furnace growth and characterisation of transition metal Heusler compounds. Talk. *DPG Frühjahrstagung, February 2008. Berlin, Germany.*

[27] A. Neubauer. Single crystal growth. Talk. *Project Meeting FOR960, Quantum Phase Transitions, May 2008. Köln, Germany.*

[28] A. Neubauer. Topological Hall effect in the A-phase of MnSi. Talk. *International Conference on Strongly Correlated Electron Systems, August 2008. Buzios, Brasil.*

[29] A. Neubauer. UHV (compatible) floating zone crystal growth of intermetallic compounds. Talk. *Deutsche Kristallzüchtungstagung, March 2008. Munich, Germany.*

[30] A. Neubauer. Vertical-zone-melting crystal growth of transition metal Heusler compounds. Talk. *Seminar of group of Prof. Elisa Baggio-Saitovitch, November 2008. Rio de Janeiro, Brasil.*

[31] J. Perlich, K. Volker, E. Metwalli, L. Schulz, R. Georgii, and P. Müller-Buschbaum. Solvent content in thin spin-coated polymer films. Talk. *DPG Frühjahrstagung, February 2008. Berlin, Germany.*

[32] C. Pfleiderer. Einkristallzüchtung unter UHV-kompatiblen Bedingungen. Talk. *Workshop der DGKK, October 2008. Frankfurt, Germany.*

[33] C. Pfleiderer. Neutron-spin-echo investigations of quantum phase transitions. Plenary Talk. *Jahrestagung der Deutschen Gesellschaft für Kristallographie, March 2008. Erlangen, Germany.*

[34] C. Pfleiderer. Non-Fermi liquid metal without quantum criticality. Invited Talk. *2nd Workshop on Novel Electronic Materials, May 2008. Kenntucky, USA.*

[35] C. Pfleiderer. Non-Fermi liquid without quantum criticality. Plenary Talk. *DPG Frühjahrstagung, February 2008. Berlin, Germany.*

[36] C. Pfleiderer. Quantum order in chiral magnets. Invited Talk. *ILL Condensed Matter Colloquium, November 2008. Grenoble, France.*

[37] C. Pfleiderer. Quantum order of chiral magnets. Plenary Talk. *Workshop on Spin Helicity and Chirality in Superconductors and Semiconductor Nanostructures, July 2008. Karlsruhe, Germany.*

[38] C. Pfleiderer. Quantum order of chiral magnets. Invited Talk. *SFB Kolloquium, July 2008. Mainz, Germany.*

[39] C. Pfleiderer. Quantum order of chiral magnets. Invited Talk. *Chez Pierre Seminar on Condensed Matter Physics at the MIT, May 2008. Massachusetts, USA.*

[40] C. Pfleiderer. Skyrmion lattice in a chiral magnet. Invited Talk. *Workshop on Competing Orders, Pairing Fluctuations and Spin-Orbit Effects in Novel Superconductors, July 2008. Dresden, Germany.*

[41] C. Pfleiderer. Skyrmion lattice in a chiral magnet. Invited Talk. *SFB Kolloquium, June 2008. Hamburg, Germany.*

[42] C. Pfleiderer. Skyrmion lattice in a chiral magnet. Invited Talk. *Workshop on Unconventional Phases and Phase Transitions, June 2008. Dresden, Germany.*

[43] C. Pfleiderer. Small angle neutron scattering and larmor diffraction in $CePt_3Si$. Invited Talk. *Workshop on Noncentrosymmetric Heavy Fermion Superconductors, May 2008. Zürich, Switzerland.*

[44] C. Pfleiderer. Spin torque effects in the skyrmion lattice of a chiral magnet. Plenary Talk. *Deutsche Neutronenstreutagung, September 2008. Garching, Germany.*

[45] C. Pfleiderer. Spin torque effects in the skyrmion lattice of a chiral magnet. Plenary Talk. *Intenational Conference for Low Temperature Physics, August 2008. Amsterdam, Netherlands.*

[46] C. Pfleiderer. Status report on intermetallic superconductors. Talk. *Workshop: How to Achieve Room Temperature Superconductivity, May 2008. Brussels, Belgium.*

[47] M. Schulz, P. Böni, E. Calzada, K. Lorenz, M. Mühlbauer, A. Neubauer, and B. Schillinger. A polarizing option for the neutron persicope. Poster. *International Topical Meeting on Neutron Radiography, September 2008. Kobe, Japan.*

[48] M. Schulz, P. Böni, E. Calzada, K. Lorenz, M. Mühlbauer, and B. Schillinger. Energy dependent neutron imaging with a double crystal monochromator. Talk. *International Topical Meeting on Neutron Radiography, September 2008. Kobe, Japan.*

[49] M. Schulz, P. Böni, E. Calzada, M. Mühlbauer, A. Neubauer, C. Pfleiderer, and B. Schillinger. Radiography with polarized neutrons. Invited Talk. *Neutrons in Science and Industry, December 2008. Garching, Germany.*

[50] M. Schulz, E. Calzada, K. Lorenz, M. Mühlbauer, and B. Schillinger. A double crystal monochromator option for ANTARES. Talk. *NEUWAVE, April 2008. Munich, Germany.*

[51] M. Schulz, C. Pfleiderer, and P. Böni. Spatially resolved neutron depolarisation measurements on $Pd_{1-x}Ni_x$. Talk. *Project Meeting FOR960, Quantum Phase Transitions, May 2008. Cologne, Germany.*

[52] R. Valicu and P. Böni. Monte Carlo simulations for focusing elliptical guides. Poster. *Deutsche Neutronentagung 2008, September 2008. Garching, Germany.*

6.5 Services to the Community

P. Böni
- Reviewer of experimental proposals, GKSS, Geesthacht, Germany.
- TUM-Beirat für den FRM II, Garching, Germany.
- Coordinator of Work Package on Neutron Optics, Joint Research Project JRA3: NMI3 FP6.
- Co-chairman of the European Workshop on Neutron Optics NOP'07, Villigen, Switzerland.
- Member of the International Program Committee of the Workshop on Polarized Neutrons in Condensed Matter Investigations (PNCMI2008), Tokai, Japan.
- Member of the Program Committee of the International Conference on Neutron Scattering (ICNS-2009), Knoxville, TN, USA.

C.Pfleiderer
- Member Beam Time Commitee, Juelich Center for Neutron Science.
- Komittee für Forschung mit Neutronen (KFN), deputy chair.
- Vertrauensdozent, Studienstiftung des Deutschen Volkes.
- Schriftführer, Verein der Freunde der Physik, TU München, e.V.

W. Häußler
- Comittee A, LLB Tables Rondes, France.

6.6 PhD Theses

Martin Engelhardt Neue Verfahren der hochauflösenden Röntgen-Computertomographie: Phasenkontrastbildgebung und Brennfleckbestimmung.

Marc Janoschek Investigation of the Chiral Magnets $NdFe_3(^{11}BO_3)4$ and MnSi by Means of Neutron Scattering.

Klaus Lorenz Implementation of Neutron Phase Contrast Imaging at FRM II.

Martin Stadlbauer Investigation of the Chemical Vicinity of Defects in Mg and AZ31 with Positron Coincident Doppler Broadening Spectroscopy.

6.7 Master's Theses

Florian Bernlochner Magnetic Structure and Excitations in the Helimagnet MnSi Studied by Neutron Scattering.

Florian Jonietz Experimentelle Untersuchung von Spin-Torque-Effekten in Helimagenten.

Christian Franz Experimentelle Untersuchung von ferromagnetischen Quantenphasenübergängen.

6.8 Zulassungsarbeiten für Lehramt

Michael Scheungraber Einführung in die physikalischen Grundlagen ausgewählter Analyseverfahren mit Neutronen und deren Nutzung in der Gemäldetiefenanalyse.

6.9 E21 Members

Phone/Fax: +49-89-289- PH: Physics Department, RS: Reactor Station

Name	Phone	Fax	Room	email
Adams Tim, diploma student	-12515	-14724	PH 1, 2373	Tim.Adams@frm2.tum.de
Bauer Andreas, diploma student	-12512	-14724	PH 1, 2367	Andreas.Bauer@frm2.tum.de
Birkelbach Felicitas, diploma student	-14515	-14724	PH 1, 2341	Felicitas.Birkelbach@frm2.tum.de
Böni Peter, Prof. Dr.	-14711	-14713	PH 1, 2215	Peter.Boeni@frm2.tum.de
Böning Klaus, Prof. Dr. emerit.	-12150	-12191	UBA 0325	Klaus.Boening@frm2.tum.de
Ceeh Hubert, diploma student	-14568	-14620	Flachbau UIL 0235	Hubert.Ceeh@frm2.tum.de
Dunsiger Sarah, Dr.	-14722	-14724	PH 1, 2207	Sarah.Dunsiger@frm2.tum.de
Franz Christian, Dipl. Phys.	-14515	-14724	PH 1, 2341	Christian.Franz@frm2.tum.de
Giemsa Stefan, mechanician	-14737	-14724	PH 1, 2341	Stefan.Giemsa@frm2.tum.de
Gläser Wolfgang, Prof. emerit.	-12476	-12474	PH 1, 2279	wglaeser@ph.tum.de
Hain Karin, bachelor student	-14568	-14620	Flachbau UIL 0235	Karin.Hain@frm2.tum.de
Janoschek Marc, Dr.	-14725	-14724	PH 1, 2214	Marc.Janoschek@frm2.tum.de
Jones Sylvia, Secretary	-14712	-14713	PH 1, 2217	Sylvia.Jones@frm2.tum.de
Jonietz Florian, Dipl. Phys.	-12512	-14724	PH 1, 2367	Florian.Jonietz@frm2.tum.de
Legl Stefan, Dipl. Phys.	-14740	-14724	PH 1, 2207	Stefan.Legl@frm2.tum.de
Löwe Benjamin, Dipl. Phys.	-12129	-14620	Flachbau 10	Benjamin.Loewe@frm2.tum.de
Mantwill Andreas, mechanician	-14887	–	–	FRM-II
Mayer Jakob, Dipl. Phys.	-12137	-14620	Flachbau 11	Jakob.Mayer@frm2.tum.de
Morkel Christoph, Dr. habil.	-14713	-14724	PH 1, 2214	Christoph.Morkel@frm2.tum.de
Mühlbauer Martin, Dipl. Phys.	-12106	-14997	RS, 125a	Martin.Muehlbauer@frm2.tum.de
Mühlbauer Sebastian, Dipl. Phys.	-12515	-14724	PH 1, 2373	Sebastian.Muehlbauer@frm2.tum.de
Neubauer Andreas, Dipl. Phys.	-12512	-14724	PH 1, 2367	Andreas.Neubauer@frm2.tum.de
Othman Osama, Dipl. Phys.	-14515	-14724	PH 1, 2341	Osama.Othmann@frm2.tum.de
Pikart Philip, Dipl. Phys.	-12161	-14620	Flachbau 10	Philip.Pikart@frm2.tum.de
Pfleiderer Christian, Prof. Dr.	-14712	-14713	PH 1, 2205	Christian.Pfleiderer@frm2.tum.de
Piochacz Christian, Dipl. Phys.	-12179	-14620	Flachbau 10	Christian.Piochacz@frm2.tum.de
Reingen Gabriel, mechanician	-12656	–	PH 1, 1321	–
Ritz Robert, Dipl. Phys.	-12515	-14724	PH 1, 2373	Robert.Ritz@frm2.tum.de
Russ Barbara, Dipl. Ing.	-14717	-14713	PH 1, 2207	Barbara.Russ@frm2.tum.de
Sandhofer Mathias, diploma student	-14515	-14724	PH 1, 2341	Mathias.Sandofer@frm2.tum.de
Schreckenbach Klaus, Prof. Dr.	-12183	-14713	PH 1, 2201	Klaus.Schreckenbach@frm2.tum.de
Schulz Michael, Dipl. Phys.	-14718	-14997	RS, 125a	Michael.Schulz@frm2.tum.de

6.10 Associated Members at FRM II

Phone/Fax: +49-89-289- PH: Physics Department, RS: Reactor Station

Name	Phone	Fax	Room	email
Calzada Elbio, Dipl. Ing.	-14611	-14997	RS, 126	Elbio.Calzada@frm2.tum.de
Georgii Robert, Dr.	-14986	-14989	NL-Halle, UYH 0336	Robert.Georgii@frm2.tum.de
Häußler Wolfgang, Dr.	-14921	-14989	NL-Halle, UYH 0334	Wolfgang.Haeussler@frm2.tum.de
Hugenschmidt Christoph, Dr.	-14609	-14620	Flachbau 9	Christoph.Hugenschmidt@frm2.tum.de
Schillinger Burkhard, Dr.	-12185	-14997	RS, 127	Burkhard.Schillinger@frm2.tum.de
Schwikowski Reinhard, technician	-14915	-14995	NL-Halle, UYH 0336	Reinhard.Schwikowski@frm2.tum.de
Wolf Alexander, mechanician	-14631	-14620	Flachbau 10	Alexander.Wolf@frm2.tum.de

6.11 Longterm Guests

Phone/Fax: +49-89-289- PH: Physics Department, RS: Reactor Station

Name	Phone	Fax	Room	email
Gähler Roland, Dr. habil.	+33-4-7620-7189	+33-4-7648-3906	Siemens AG	gahler@ill.fr
Keller Thomas, Dr.	-12164	-14997	RS, 106	Thomas.Keller@frm2.tum.de
Vollmer, Nico, Dr.	+49-9131-1893018	+49-9131-1894705	Fuel Europe Engineering Materials	nico.wieschalla@areva.com
Niklowitz Philipp, Dr.	+44-1784-44-3499	–	–	philipp.niklowitz@rhul.ac.uk
Chabior Michael, Dipl. Phys.	+49-89-36351042	–	Siemens AG	Michael.Chabior.ext@siemens.de

6.12 Short-term Scientific Visitors

Name	Institute	Duration of stay
Duncan Will[1]	Royal Holloway, UK	Sept-Oct. 2008
Koenigs, Jörgen	TU Delft	Oct 2008 - Feb 2009

[1] European Community, COST P16

6.13 Guided Tours at FRM II

The FRM II is open for everybody to come and visit the scientific and experimental facilities (Experimental Hall and Neutron Guide Hall). Therefore, Guided Tours are organized by a specially established division, the „Besucherdienst“, and conducted by the scientists and the technical personnel of FRM-II.

In 2008, the members of E21 guided approx. 140 officially registered tours and several others at various occasions, thus contributing a significant amount of time and personal effort to help making the Neutron Source FRM-II a publically transparent and accepted research facility.

6.14 Third Party Funding

We gratefully acknowledge financial support from

- Deutsche Forschungsgemeinschaft (DFG)
- Bundesministerium für Bildung und Forschung (BMBF)
- European Community: COST-P16 Program
- European Community: NMI3 Program
- Bavaria California Technology Center (BaCaTeC)
- Deutscher Akademischer Austauschdienst (DAAD)
- Swiss National Science Foundation (SNF)

We also acknowledge beam time at:

- European Synchrotron Radiation Facility (ESRF)
- Hahn-Meitner-Institut (HMI)
- Institut Laue-Langevin (ILL)
- Paul-Scherrer-Institut (PSI)

1	F. Repper	10	J. Mayer	19	P. Pikart	28	K. Schreckenbach
2	A. Wolf	11	F. Jonietz	20	T. Merz	29	C. Hugenschmidt
3	K. Hain	12	C. Piochacz	21	R. Ritz	30	M. Janoschek
4	S. Dunsiger	13	E. Calzada	22	C. Morkel	31	C. Pfleiderer
5	S. Jones	14	A. Neubauer	23	C. Franz	32	S. Mühlbauer
6	B. Russ	15	H. Ceeh	24	S. Legl	33	T. Adams
7	A. Komarek	16	M. Mühlbauer	25	M. Rahn	34	S. Giemsa
8	A. Bauer	17	B. Schillinger	26	P. Böni		
9	M. Schulz	18	*Guest*	27	R. Georgii		

Missing: F. Birkelbach, K. Böning, W. Gläser, B. Löwe, A. Mantwill, O. Othman, M. Sandhofer, W. Häußler, R. Schwikowski

E21 Gallery

E21 relaxing after a long day at the DPG Frühjahrstagung.

Andi and Stefan enjoying their food at the cantina at CBPF in Rio de Janeiro...

... while others are waiting for better times to come.

E21 Positron group after a hiking tour.